State Dependency of Beta Oscillations in the Cortico-Basal-Ganglia Circuit and their Neuromodulation under Phase Locked Inputs

Timothy O. West[1,2,3], Simon F. Farmer[4], Peter J. Magill[2,5], Andrew Sharott[2], Vladimir Litvak[3], Hayriye Cagnan[1,2,3]

[1.] *Nuffield Department of Clinical Neurosciences, John Radcliffe Hospital, University of Oxford, Oxford*

[2.] *Medical Research Council Brain Network Dynamics Unit, University of Oxford, Oxford, OX1 3TH, United Kingdom.*

[3.] *Wellcome Trust Centre for Human Neuroimaging, UCL Institute of Neurology, Queen Square, London, WC1N 3BG, UK.*

[4.] *Department of Neurology, National Hospital for Neurology & Neurosurgery, Queen Square, London WC1N 3BG, UK.*

[5.] *Oxford Parkinson's Disease Centre, University of Oxford, Oxford OX1 3QX, United Kingdom.*

**Corresponding Author*

Abstract

Currently employed strategies for therapeutic brain stimulation take a static approach to determining stimulation parameters. However, it is well understood that brain states fluctuate over time, depending for instance upon differing behavioural or disease states. Here, we characterize the impact of changes in connectivity upon the emergence of rhythmic neural activity in the circuits formed by the cortex, basal-ganglia, and thalamus. Importantly, we show how the efficacy of interaction with these rhythms via phase-specific stimulation is highly dependent upon the current network state. We take a computational approach to do this, modelling the population activity of the cortico-basal ganglia-thalamic circuit and fitting model parameters to match the spectral features of empirical data obtained from a 6-OHDA lesioned rat model of Parkinson's disease. Using this fitted model, we then dissect the role of the circuit's multiple loops in the maintenance of subcortical beta rhythms and their synchronization. We show that a competition of cortical and striato-pallidal inputs to the subthalamic nucleus , a main input hub of the basal-ganglia, determines the frequency, amplitude, and timing of

beta band (14-30 Hz) activity. In addition, we demonstrate how the efficacy of cortical inputs in modulating ongoing subthalamic beta activity is dependent upon their relative phase alignment- with their precise effects in turn determined by the connectivity state of the network. These results inform our understanding of: (a) how alterations in circuit connectivity can lead to the emergence of pathologically amplified rhythms; (b) how precisely timed phasic stimulation can be leveraged to modulate aberrant brain activity; and (c) how effective stimulation parameters depend on the "connectivity state" of the circuit; highlighting the importance of incorporating an estimation of brain state in the determination of optimum stimulation parameters.

Keywords

Parkinson's disease, basal ganglia, phase-locked stimulation, closed-loop brain stimulation

Introduction

Therapeutic brain stimulation, such as continuous deep brain stimulation (cDBS) for Parkinson's disease (PD), currently adopts a static approach to the control of its delivery. Stimulation parameters are set fixed in the clinic in order to maximize the reduction in patient's symptoms while at the same time minimizing adverse side effects (Volkmann et al., 2009). cDBS suppresses aberrant neural oscillations that emerge during so called 'oscillopathies' (Llinás et al., 1999; Brown et al., 2001; Dostrovsky and Bergman, 2004; Uhlhaas and Singer, 2006; Brittain and Brown, 2014). For example, in dopamine depleted states associated with PD, oscillatory activity in the beta frequencies (14-34 Hz), normally engaged during the functional control of movement (Engel and Fries, 2010; Jenkinson and Brown, 2011; Khanna and Carmena, 2015; Palmer et al., 2016), becomes abnormally amplified across the circuits formed by the cortex, thalamus, and basal-ganglia (Brown et al. 2001; Levy 2002; Mallet et al. 2008b; Weinberger et al. 2006). These rhythms are widely synchronized (Sharott et al., 2005; de Solages et al., 2010; Litvak et al., 2011; Delaville et al., 2014; West et al., 2016, 2018) with a frequency and amplitude modulated by specific brain states such as rest, movement, movement planning, sustained contraction, decision making, action planning, and anaesthesia (van Wijk et al., 2012; Brazhnik et al., 2014).

Neural activity in the beta frequencies exhibit intermittent fluctuations, consisting of high-amplitude sub-second events which are referred to as 'bursts' and have been characterised in both pathological (Tinkhauser et al., 2017b; Torrecillos et al., 2018; Cagnan et al., 2019b) and functional (Feingold et al., 2015; Lundqvist et al., 2016; Khanna and Carmena, 2017; Shin et al., 2017; Little et al., 2019) brain activity. Recent experiments have demonstrated that these rhythms can be specifically interrupted using adaptive DBS (aDBS) (aDBS; Little et al., 2013; Arlotti et al., 2016; Tinkhauser et al., 2017a)- a novel control algorithm that triggers stimulation at the onset of a beta burst. Importantly

the timing of the delivery of brain stimulation has important impacts on behaviour (Stagg et al., 2011; Pirulli et al., 2013; Martin et al., 2014; Herz et al., 2018) indicative of state dependent efficacy (Silvanto et al., 2008). Therefore, understanding of how timing of activities within these circuits changes between different brain states, could help provide more nuanced targeting of stimulation (McIntyre and Hahn, 2010; Cagnan et al., 2019a).

Understanding the timing of subcortical beta bursts and optimal strategies for their suppression requires a systems approach to inferring the mechanisms involved in their generation, propagation, and maintenance. Several circuits have been invoked- such as the pallido-subthalamic feedback (Bevan et al., 2002; Terman et al., 2002; Cruz et al., 2011; Tachibana et al., 2011; Liu et al., 2017; Shouno et al., 2017); cortico-basal-ganglia thalamic 'long loop' (Pavlides et al., 2015; Brazhnik et al., 2016); the thalamocortical relay (van Albada et al., 2009; Reis et al., 2019); changes in striatal outflow (Gillies and Willshaw, 2004; Brown, 2007; Hammond et al., 2007; Kumar et al., 2011); or intrinsic striatal dynamics (McCarthy et al., 2011). It is likely that the observed activity arises from a competition between these circuits (Leblois et al., 2006; Pavlides et al., 2015; Fountas and Shanahan, 2017) with the propagation of activity across different loops predominating during particular network states. The positioning of the subthalamic nucleus (STN) as site of convergence for many of these pathways makes it a prime candidate for playing a focal role in the functional anatomy of the network (Mastro and Gittis, 2015; Deffains et al., 2016) as well as a primary target for neuromodulation (Haynes and Haber, 2013).

A systems approach to understanding the mechanisms of pathological oscillations invokes notions of changes in the relative timing of activities between disparate brain regions (Cagnan et al., 2015, 2019b), thought also to be important for healthy communication in the brain (Womelsdorf et al., 2007; Fries, 2015). In order to specifically disrupt synchronization of pathological brain rhythms, novel stimulation strategies have been developed which aim to deliver stimulation phase-locked to an ongoing control signal such as the peripheral tremor amplitude (Brittain et al., 2013; Cagnan et al., 2017) or STN beta activity (Holt et al., 2019; Peles et al., 2019; Sanabria et al., 2020). In line with this, recent experimental work has demonstrated that phase locked stimulation is a viable method for modulating both neural activity and behaviour (Polanía et al., 2012; Siegle and Wilson, 2014; Cordon et al., 2018; Zanos et al., 2018; Peles et al., 2019).

In this work we use a computational model of the cortico-basal-ganglia-thalamic network (Moran et al., 2011; Marreiros et al., 2013; van Wijk et al., 2018) that has been fit (West et al., 2019a) to intracranial recordings made in 6-OHDA lesioned rat model of Parkinson's disease (Mallet et al., 2008b). This model demonstrates that rhythmic activity within this circuit is the manifestation of an interplay between reciprocal cortico-basal ganglia loops. Furthermore, these rhythms can be manipulated using precisely timed, phase locked stimulation of the cortex or STN. We investigate the

interaction between state dependent changes in the expression of beta rhythms and the efficacy of phase locked stimulation to better inform how adaptive stimulation control can provide consistent therapeutic effects in the face of spontaneous changes in brain networks.

Materials and Methods

Model Optimization with Approximate Bayesian Computation

This study reports an analysis of a computational model of the cortical-basal-ganglia-thalamic circuit. In a previous paper we reported a model optimization and model selection procedure based upon the Approximate Bayesian Computation framework (ABC) (West et al. 2019a). This procedure was used to fit 13 different models of the network to empirical data, and then subsequently select the candidate model that could best explain its spectral features. For a full formulation of the fitting procedure please see West et al. (2019a). Briefly, ABC provides a likelihood free optimization algorithm (Beaumont et al., 2002; Liepe et al., 2014) that is founded in the generation of 'pseudo-data' from numerical simulations of a model that can then be compared to the empirical data using a common set of features (e.g. spectral power). By gradually reducing the distance between a set of data features common to the empirical data and pseudodata through the optimisation of model parameters, the algorithm may converge on an approximation to the posterior distribution over parameters of the model (i.e. the parameters of the model that best explain the observed data). ABC allows for causal models of steady state features such as spectra to be modelled without placing any restrictions on the temporal dynamics that give rise to them. In this way we can explore transient dynamics such as beta bursts in post-hoc analyses of fitted models. In this study, we used each population's local oscillatory profile (i.e. the power spectra) plus the patterns of connectivity between them (i.e. the directed functional connectivity). To determine directed functional connectivity, we used non-parametric directionality (NPD; Halliday et al., 2016; West et al., 2019b).

Model Description

We employ a model formalism that is based upon a description of the propagation of activity across the neural populations of the cortico-basal-ganglia-thalamic network. Specifically we use a system of coupled neural mass equations (Jansen and Rit, 1995; David and Friston, 2003) to simulate the distributed activity across this network. The biological and theoretical basis of this model has been described previously (Moran et al., 2011; Marreiros et al., 2013; van Wijk et al., 2018). Furthermore, we adapt the original state equations to incorporate stochastic inputs and explicity, finite transmission delays. For the full state space description of the model and technical details regarding the integration of the state equations, please see the supplementary methods. Overall the model consists of nine coupled 2nd order stochastic differential equations, each modelling a separate (assumingly homogenous) population of neurons within the circuit. This includes a model of the motor cortex consisting of three pyramidal layers plus an inhibitory interneuron population (Bhatt et al., 2016); the

striatum (STR); the external and internal segments of the globus pallidus (GPe/i); the subthalamic nucleus (STN); and the thalamus (Thal.).

In this paper we bring forward the posterior model fit from West et al. (2019a) where we used ABC to fit 13 variations of the full model that included or excluded different key connections such as the subthalamo-pallidal feedback (STN → GPe) and the hyperdirect pathway (M2 → STN). We then used a model comparison approach to determine a subset of these models as the best explanations of the empirical data, accounting for both the individual model's ability to accurately reproduce the observed data and the extent to which model parameters deviate from a prior distribution (detailed in table 3 of the supplementary methods).

After discounting for difference in the parsimony of posterior model fits (i.e. the divergence between posterior and prior distributions over parameters), we found that a model incorporating both the hyperdirect and subthalamo-pallidal pathways was the best candidate in describing the patterns of pathological activity in the 6-OHDA lesioned rat. This posterior model fit is used for the simulations in this paper which we refer to as the *fitted* or *base* model and its structure is presented in figure 1.

Empirical Data – 6-OHDA Lesioned Rats

The models were fitted to archival data consisting of multisite recordings in the basal ganglia and cerebral cortex of rats with a 6-hydroxydopamine (6-OHDA) induced dopamine depletion of the midbrain- a lesion model of the degeneration associated with Parkinsonism in humans (Magill et al., 2004, 2006). These animals were implanted with two electrodes to measure local field potentials (LFP) from multiple structures in the basal ganglia: dorsal striatum, GPe, and STN. Additionally electrocorticography was measured over area M2 of the motor cortex, a homologue of the Supplementary Motor Area (SMA) in humans (Paxinos and Watson, 2007). Animals were recorded under isoflurane anaesthesia and during periods of 'cortical-activation' (Steriade, 2000) induced by a hind-paw pinch. For more details of the experimental recordings and their acquisition please see the original experimental papers (Magill et al., 2004, 2006).

Preprocessing of time series data (both LFP and ECoG) were done as follows: 1) all data were first downsampled from the hardware native 17.9 kHz to 250 Hz using Spike2 acquisition and analysis software (Cambridge Electronic Design Ltd., Cambridge, UK); 2) imported into MATLAB; 3) mean subtracted; 4) band-passed filtered 4-100 Hz with a finite impulse response, two-pass (zero-lag) with filter order optimized for data length; 5) Z-scored to standardize to unit variance; and 6) subjected to a Z-score threshold criterion such that epochs containing any high amplitude artefacts were removed. The exact threshold was chosen on a case by case basis dependent upon recording gain and size of the artefact. This artefact-rejected, epoched data was then taken forward to compute the autospectra and NPD used as features for the ABC fitting procedure.

Spectral Estimation of Empirical and Simulated Data

Analysis of simulated and empirical data involved computation of power spectra. Power spectra were constructed using the averaged periodogram method across 1 second epochs and using Hanning tapers. For the empirical power spectra (used only for fitting the ABC models), 1/f background noise was removed by first performing a linear regression on the log-log spectra and then subtracting the linear component from the spectra. This ensured that the parameter estimation scheme was focused upon fitting the spectral peaks in the data and not the profile of 1/f background noise.

To compute functional connectivity (magnitude squared coherence; used only in the analysis of the post-hoc simulations) and directed functional connectivity (NPD; used only as a data feature in the ABC fitting) we used the Neurospec toolbox (http://www.neurospec.org/), again using 1 second epochs. Features in the empirical data were fit using a sum of Gaussians (maximum of three), with order optimized using adjusted R^2. This was done to smooth the data features to aid the fitting procedures.

Inactivation Simulations and Sweeping of Connection Strengths

In the first set of simulations we perform a systematic inactivation analysis to determine which connections are required for the generation and/or propagation of beta oscillations in the STN in the fitted model. This was done by taking the fitted model and removing connections from the model by setting their strengths to zero. We then re-simulate the data and compare the resulting power/magnitude and frequency of the power and coherence with that of the original model in order to determine a percentage change in beta amplitude. We define the power as the sum within the beta band from 14-30 Hz, divided by the number of frequency bins, magnitude as the peak value of coherence within the band and take the frequency as the peak of the spectra within the band. In some cases we also define lower (14-21 Hz) or upper (21-34 Hz) beta frequency bands.

In some sets of simulations, we sweep across different connection strengths to investigate their impact on network dynamics. We simulate models with strengths of connections ranging from 10% to 190% of the parameter inferred from the empirical data. The (signed) connection strength of the nth connection C_n is given by:

$$C_n = P_n \times \exp(K_n)$$

Equation (1)

with P_n as the expected value of the posteriors of the fitted model (detailed in table I of the supplementary methods). Individual connection strengths are reported both as the percentage deviation from the fitted value; as well as their log scaling parameter (K_n).

Analysis of Reciprocal Circuit Activity in the Maintenance of Beta Power and Cortico-Subthalamic Beta Coherence

To investigate how differences in the strengths of loops within the circuit impact the steady state (i.e. the time averaged) properties of beta synchrony within the network, we set up an analysis in which we simulated models with random connectivity. To simulate these models, we drew 500 sets of connectivity parameters from the posterior distribution of the empirical model. In order to increase the range of connectivity that was analysed, we artificially inflated the spread of the posterior distributions by doubling their variances prior to this draw. All other parameters were held fixed at the values specified in the posterior of the fitted model (detailed in supplementary information). For each random model, 30 seconds of data was simulated, and the spectral properties were estimated (see Spectral Estimation of Empirical and Simulated Data). We exclude simulations that are either exponentially divergent or perfectly periodic (see supplementary methods) to restrict model dynamics to yield intermittent behaviour. To summarise the connectivity within each model we derive two measures:

1) A measure of the sum of absolute connection strength (disregarding the sign of the connection):

$$NetC = \sum_{N}^{i=1} |C_n|$$

Equation (2)

where C_n is the connection strength of the nth connection. This is then reported as a percentage difference from the mean of the simulated set. This measures the total degree of connectivity within the loop irrespective of whether it comprises inhibitory or excitatory connections. We refer to this as *net loop strength*.

2) In order to measure differences in circuitry arising from either a net increase in excitation or inhibition, we also derive a measure of the E/I balance within a loop:

$$NetEI = \sum_{N}^{i=1} C_n$$

Equation (3)

We report this as a difference from the mean of the simulated set. By accounting for the sign of the connection this measure yields the net change in the relative excitation or inhibition within the loop. We refer to this as *net loop E/I balance*.

Using these two measures we then estimate how both change between models yielding either the 1st and 4th quartiles of STN beta (14-30 Hz) power, M2 beta power, and STN/M2 beta coherence.

Differences in loop strength associated with these two model sets are estimated using Student's t-test, and statistical significance established using a Bonferroni corrected significance threshold. We also test for the correlation of loop connectivity measures (1) and (2) with power and coherence. In the case that the non-parametric (Spearman's) correlation test reached (Bonferroni corrected) significance level, we computed linear regressions of the relations.

Definition of Burst Events and their Timings

To characterize the properties of intermittencies in rhythms within the simulated data, we follow a similar approach to that taken in previous experimental work (Tinkhauser et al., 2017b) that constructs a band filtered signal and uses a threshold to define burst events as suprathreshold amplitude activity. In this case we use a two-pass, Butterworth filter with a passband of 18±7.5 Hz. We take the Hilbert transform of this narrowband series to compute the analytic signal. The amplitude envelope of this signal is then taken as the absolute value of the transform. From this signal we can then define a threshold to determine burst events. In this application we use the 75th percentile of the data. Note that when comparing bursts across different simulations we concatenate simulated data in order to determine a burst threshold from the joint space. Each population has its own threshold determined by the concatenated data. Bursts were only determined significant if they had a total duration longer than at least 1.5 cycles of an 18 Hz oscillation (middle of the passband) equivalent to 83 ms.

In order to look at the dynamics that occur within and around burst initiation, maintenance, and termination we performed a time-locked analysis of the evolution of the simulated signals. In order to determine the relative timing of beta rhythms across the network, we use the threshold crossing (determined as above) of an amplitude envelope from a given population as the set point by which to temporally align the data. By looking at the relative timing of bursts occurring across the remaining population (estimated via the median onset/offset time across all bursts) we can then elucidate the changes in the circuit that occur prior to the onset of a burst in a given reference population. This can be used to determine a sequence of changes in the beta amplitudes of each population that preclude the onset and termination of a burst at the reference. Furthermore, we alter the strength of inputs to the STN to determine how connectivity can dictate the temporal ordering of this sequence of events. For the main set of results presented in figure 5 we use the STN as the population by which to time-lock the analysis. In order to prevent large but temporally distant bursts from interfering with estimations of timings, we applied a Hanning window to the period ±300 ms either side of the STN onset. Differences in the timings of burst onsets and offsets with respect to the reference population were computed using two sample t-tests and Bonferroni corrected for multiple comparisons.

A supplementary analysis was also made to determine the proportion of coincident bursts. This was done by computing the proportion of bursts in each population that were detected simultaneously within a window ±300ms of the onset of the reference burst.

Simulating Closed Loop Stimulation of Motor Cortex or STN with Input Phase Locked to Beta Burst Activity

To determine how the effects of precisely timed inputs to the network shape ongoing activity we performed a set of simulations giving stimulation to one receiving population triggered and phase locked to beta burst activity in a reference population. We first simulated a baseline set of data (100s in

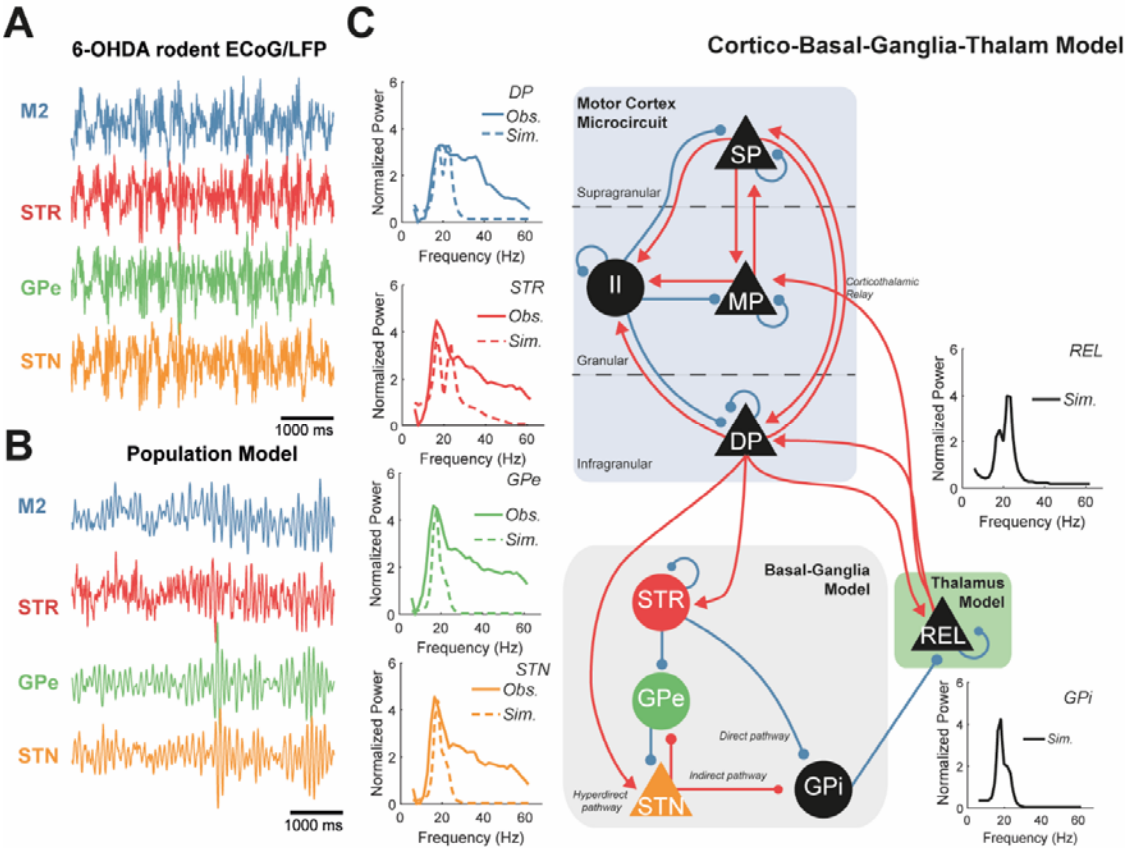

Figure 1 – **Schematic of cortico-basal ganglia-thalamic model and fit to empirical data from Parkinsonian rodents.** A model of the population activity in the circuit was fitted to data features (power spectra and functional connectivity) of **(A)** electrophysiological recordings (electrocorticography at M2 + local field potentials from striatum STR; external segment of the globus pallidus GPe; and the subthalamic nucleus STN) made in 6-OHDA lesioned rat model of Parkinson's disease (procedure detailed in West et al. 2019a). **(B)** This model yields time series with transient, burst like behaviour similar to that seen in vivo. **(C)** This schematic details the coupling of excitatory (glutamatergic; triangles) and inhibitory (GABAergic; circles) populations and their corresponding projections. A cortical source is modelled using a three layer microcircuit (Bhatt et al., 2016) comprising three layers: superficial pyramidal cells (SP; supragranular); middle pyramidal (MP; granular); and deep pyramidal cells (DP; infragranular), plus a global inhibitory interneuron population (II). The basal ganglia comprises four subpopulations modelling activity in the STR, GPe, STN, and internal segment of the pallidus (GPi). The GPi forms the output of the basal ganglia and acts to inhibit relay cells (REL) of the thalamus. The main subcortical pathways annotated include the direct, indirect, hyperdirect, and thalamocortical relays. The inset graphs indicate the empirical and simulated power spectra in bold and dashed respectively. GPi and REL are treated as hidden nodes and their respective neural activities are inferred from dynamics of other brain regions.

duration) from the fitted model and then identified bursts using the procedures described in section Definition of Burst Events and their Timings. We then re-simulated the model with an identical noise process and added an additional input manipulated to have a fixed phase relation with respect to activity in either the STN or motor cortex. This input was triggered to the onset of bursts in the reference (in the base data and again at the 75th percentile of the amplitude envelope) to deliver 300ms of stimulation.

In order to derive the phase-locked stimulation waveform we derived the analytic phase of the reference activity from the argument of the Hilbert transform to yield $\phi_{REF}(t)$. The stimulation to the cortex was then given by: $Stim = A \sin(\phi_{REF}(t) + \Delta\phi)$ where $\Delta\phi$ sets the relative phase of the stimulation with respect to the reference. A is the amplitude and was fixed to yield ¼ of the variance of the input noise to the stimulated population. In cases where cortex was stimulated, exogenous input was delivered to the middle layer of the cortex. . Overall, the phase was swept from -π to +π radians in 12 bins. The resulting power spectra for each stimulation regime was analysed and plot against phase to yield bandlimited amplitude response curves (ARCs) in either lower (14-21 Hz) or upper (21-34 Hz) beta bands.

Finally, the changes in burst patterning following phase locked stimulation were quantified by analysing the burst rates, amplitudes, durations, and intra-burst cortico-subthalamic phase synchrony (measured using Pairwise Phase Consistency *PPC*; Vinck et al., 2010). These were measured for each stimulation setting, and then plot against the relative phase of the stimulation.

Determining State Dependency of Phase Locked Stimulation of Motor Cortex

In a final set of simulations we investigate how the amplitude response curves pertaining to the phase locked stimulation of the motor cortex relative to STN are determined by the connectivity state of the circuit. To do this we perform the same simulation and analysis as above but modulate the strength of connectivity of the hyperdirect and pallido-subthalamic pathways. The percentage change in amplitude from the median is then used to plot the ARC. We summarise changes to the ARC by reporting the minimum, maximum, and range and then plotting these against the strength of connectivity.

Results

Results of Model Fitting to Electrophysiology of Parkinsonian Rats

Electrophysiological recordings made in a 6-OHDA rat model of PD were used to constrain a biophysically plausible model of population activity in the cortico-basal-ganglia-thalamic circuit using a procedure previously reported in West et al. (2019a). The details of this circuit model and its resulting empirical fits are presented in figure 1. Fitting was used to optimize model parameters in order to best explain the observed local oscillatory dynamics at each population estimated via their autospectra, as well as the interaction between them as measured using functional connectivity. Several empirical

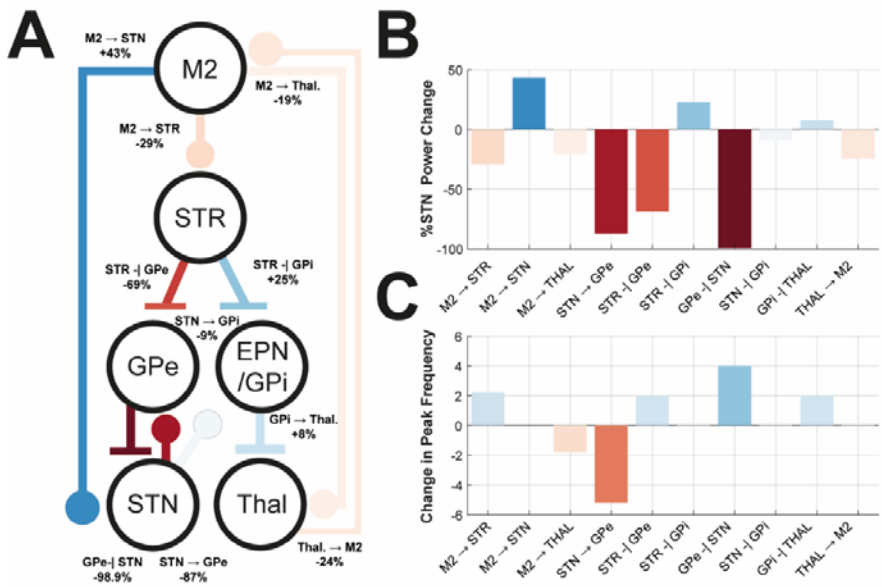

Figure 2 – **Simulated inactivation experiments to determine the contribution of individual connections in the cortico-basal-ganglia-thalamic circuit to the origin of STN beta oscillations.** Connections in the fitted model were individually removed and the resulting change in beta power measured. **(A)** Schematic of the results of the simulated inactivation experiments. Connections are colour coded to indicate the change in 14-30 Hz beta power in the STN (red or blue indicating a reduction or increase following lesion, respectively). The actual percentage change is annotated alongside each connection. **(B)** Bar plot of the changes in STN beta power from the base model following inactivation of each connection. **(C)** Bar plot of the changes in STN peak frequency from the base model (within the beta band) following inactivation.

features of the data were well reproduced by the fitting procedure such as 1) the widely synchronized beta oscillation across the network (figure 1B; inset); 2) significant feedback of beta oscillations from subcortex to cortex. Model fits did not well reproduce higher frequency activity (>30 Hz) found in the empirical data (figure 1B; inset); 3) bursting behaviour similar to that seen in traces recorded in vivo (figure 1A and C). The remainder of the results in this paper explore the dynamics of the fitted model (i.e. the base model with parameters detailed in table 3 of the supplementary methods), and how changes in connectivity and input induce changes with respect to it.

In-silico Inactivation Experiments: Cortico-Basal-Ganglia-Thalamic Connectivity Determines the Power of Subthalamic Beta Rhythms

We performed a set of in-silico inactivation experiments in order to determine how connectivity within the cortico-basal ganglia-thalamic circuit can lead to emergence of pathological beta rhythms in the subthalamic nucleus (STN). Connections in the model were systematically removed and the resulting changes in beta power in the STN were analysed. In figure 2A, the changes in STN beta power resulting from the removal of a connection are shown. When summarised in the bar graphs in figure 2B, four out of ten connections act to significantly promote STN beta oscillations (i.e. a greater

than 25% post-lesion loss in power). Removal of connections in the indirect pathway (M2 → STR: -29%; STR → GPe: -

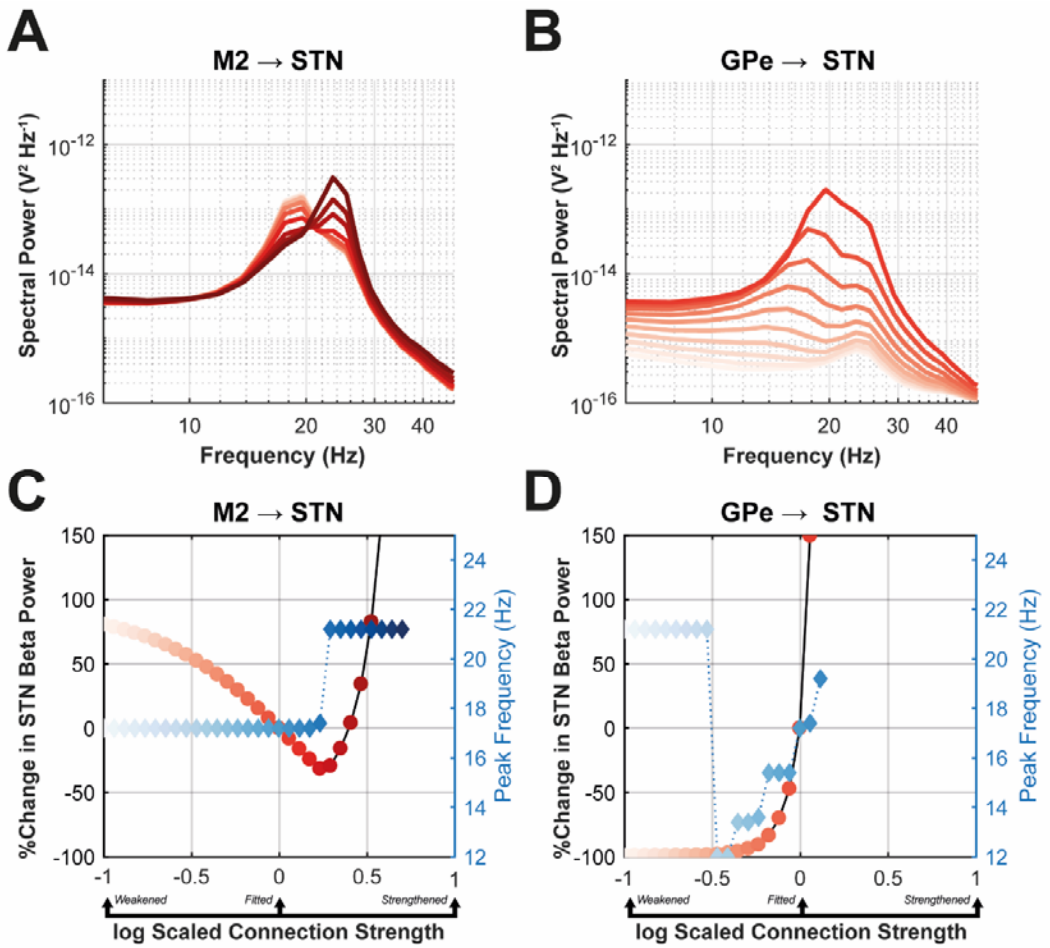

Figure 3 – **The effects of modulating the strength of STN inputs from the excitatory hyperdirect projection (M2 → STN) and inhibitory pallido-subthalamic projection (GPe → STN) upon the power spectra of STN population activity.** The strengths of the two connections were varied independently (1st column- hyperdirect; 2nd column- subthalamo-pallidal) and data was simulated (500 s) from the resulting models. The fitted connection strength for the base model is denoted as 0%. **(A)** The power spectra of the STN resulting from a modulation of 10% to 300% of the fitted connection strength of the hyperdirect connection (colour coded such that red indicates stronger connection). Modulating this connection exposes a bistability between a low beta (< 20 Hz) and high beta (> 21 Hz). **(B)** Same as (A) but for the subthalamo-pallidal connection. Increasing the strength of this connection raises the frequency and amplitude of beta. **(C)** Plot of peak beta amplitude (left axis) and peak beta frequency (right axis) under modulation of hyperdirect input. The switch from low to high beta occurs at 0.2 (equivalent to 160% of the fitted connection strength). **(D)** Same as (C) but for pallido-pallidal connection. The modulation of STN power is monotonic, increasing with heightened STN inhibition from the pallidum.

69%; GPe → STN -99%; and STN → GPe: -87%) was found to result in weakening of beta rhythms. The thalamocortical relay was found to weakly promote beta rhythms (19-24% reduction post-lesion).

Overall, pallido-subthalamic inhibition was the most critical connection for maintenance of STN beta oscillations (99% reduction post lesion). The excitatory and inhibitory connections from the STN and GPe respectively, act to either increase (4 Hz increase post-lesion) or decrease (5 Hz reduction post-lesion) the frequency of the beta peak frequency (figure 2C).

In contrast, two connections have suppressive effects on STN beta power in the base model (i.e. a greater than 25% post-lesion increase in power). Blue connections in figure 2A indicate that beta power increased after inactivation of the direct pathway (STR → GPi/EPN: +25%) and hyperdirect pathway (M2 → STN: +43%). The basal ganglia output pathway (GPi → Thal.: + 8%) was responsible for only a weakly suppressive effect and its influence is likely determined by the balance of converging inputs from direct/indirect pathways. Removal of the hyperdirect pathway does not change the peak frequency of STN beta in the base model (figure 2C).

We have identified two connections in the model that yield either the largest promotion (GPe → STN; pallidal-subthalamic inhibition) or suppression (M2 → STN; hyperdirect pathway) of STN beta oscillations following their removal. Both connections converge at the STN and the majority of the following results will focus upon simulations investigating modulation of these pathways.

Cortical and Pallidal Inputs to the STN Induce Transitions in the Spectral Power and Frequency of Beta Oscillations

Next we investigated how transitions in STN beta power are dictated by the strength of input from cortex and pallidum. In figure 3A, simulated spectra are shown for when the hyperdirect pathway strength (M2 → STN) was altered from the base model (K = -1 to +1). As before, weakening of the M2 → STN connection increases the amplitude of low frequency beta. However, strengthening the hyperdirect pathway greater than that of the fitted value (i.e. strengths at K > 0) exposes a switching behaviour in the model (figure 3C) that induces a transition between lower beta frequencies (< 21 Hz) and upper beta frequencies (21-34 Hz) at K = 0.2 (equivalent to 160% of the strength of the connection in the fitted model). Beta power is minimum close to this switching point. At connection strengths greater than K = 0.7, the model enters a 'non-physiological' regime reflecting an exponentially divergent state; connectivity yielding very large spectral powers ($>10^{-12}$) are excluded from all further analyses. A similar relationship was found when analysing the effects of hyperdirect pathway upon power in the motor cortex (see supplementary information I) where a switch to high beta activity in the motor cortex with an increase in hyperdirect strength.

We next modulated the strength of the GPe → STN connection (figure 3B and D) and demonstrated that increasing STN inhibition shifts beta to higher amplitudes and lower frequencies. In figure 3B we demonstrate that this transition to lower frequency activity (> 12 Hz) occurs at K > 0.5. Above this point, STN beta power increases exponentially. Strengthening the inhibition above 125% of the fitted

strength results in a non-physiologically plausible state (defined as above). Again, the empirically fitted connection strengths of this pathway (K = 0) are close in proximity to the transition point. Beta power

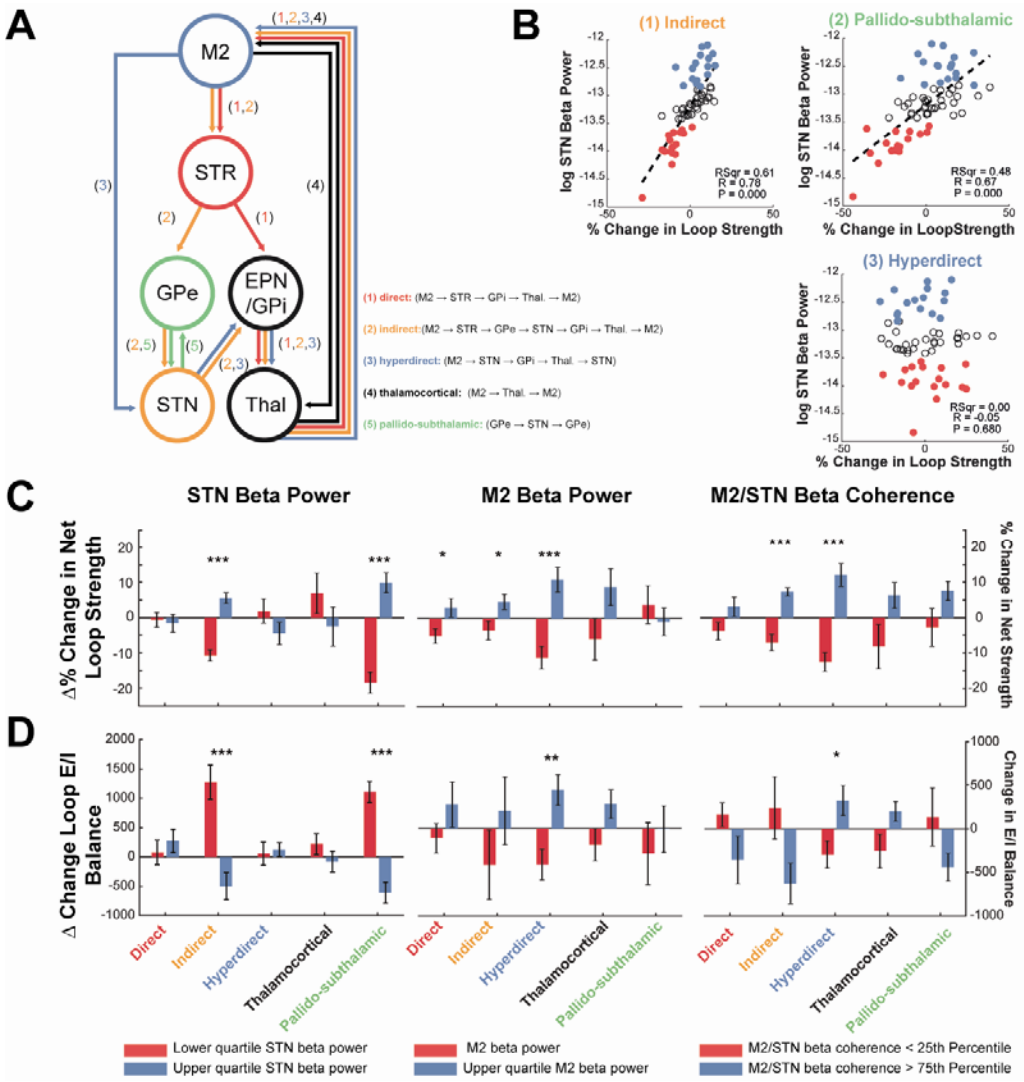

Figure 4 – **Contributions of loops within the cortico-basal-ganglia-thalamic circuit towards the expression of heightened beta power in the STN and motor cortex, and cortico-subthalamic functional connectivity.** 500 models were generated by drawing connectivity parameters from the (inflated) posterior distributions of the empirical model. These models were then simulated for 30s and the spectral properties of their outputs analysed. **(A)** Circuit diagram indicating the various loops under investigation: direct, indirect, hyperdirect, thalamocortical, and pallido-subthalamic loop. The individual connections contributing to each of the five loops are annotated by the numbers alongside. **(B)** Scatter plots of *loop strength* vs the resulting STN beta power. Samples in the upper and lower quartiles of beta power are marked in blue and red respectively. Where there was significant correlation (Spearman's coefficient; Bonferroni corrected $\alpha^* = \alpha/n$; where n = 15 separate tests) a linear regression is plot and resulting statistics inset. This is a selection of graphs- for the full results please see supplementary information III. **(C)** Bar graphs of the mean *loop strength* associated with models yielding strengths of STN beta (14-30 Hz) power, M2 beta power, and STN/M2 coherence below or above the 1st and 4th quartiles (red and blue respectively), and in the first, second, and third columns respectively.

Differences in connectivity were tested using student t-tests with Bonferroni corrected significance thresholds ($\alpha^* = \alpha/n$; where n = 30 separate tests). Error bars give the standard error of the mean. **(D)** Same as (C) but estimating differences in *excitation/inhibition balance*.

in the motor cortex (supplementary information I) yielded a similar response to the STN, with increasing pallidal inhibition inducing a shift to lower frequencies and exponentially increasing power.

The Thalamocortical Feedback is Necessary for the Promotion of Low Frequency Beta Activity

A set of simulations were performed to investigate how the: (A) corticothalamic projection; (B) thalamocortical return; and (C) the projection from GPi to thalamus impacted cortical beta power. The cortical-thalamic return is largely responsible for the promotion of lower frequency (< 21 Hz) beta from the basal ganglia as blocking this causes almost complete attenuation of beta in M2 (supplementary figure V). In the case that direct cortical input to the thalamus is inactivated, cortical rhythms are biased towards low frequency activity propagating from the GPi.

Functional Connectivity of the STN and Cortex is Nonlinearly Related to Coupling Strength

The efficacy of connections within the network also modulates inter-regional functional connectivity between the cortex and STN estimated with coherence (see supplementary information II). These effects mirror those seen when looking at power, with frequencies biased to either higher or lower frequency beta ranges dependent upon the strength of inputs to the STN from cortex and GPe respectively. However, the relationship between coherence and hyperdirect pathway strength is non-monotonic: at K = 0.2 (equivalent to ~160% of the fitted value) coherence is at its peak (+10% from the fitted value), weakening or strengthening the M2 → STN pathway from this point reduces the magnitude of coherence. Strengthening the connection to the maximum (K = 0.7 equivalent to 165% of the fitted strength) reduces STN/M2 coherence by over 25%. This data can help reconcile the paradoxical findings that dopamine depletion can lead to synaptic weakening of glutamatergic inputs to the STN (Mathai et al., 2015a; Chu et al., 2017) whilst at the same time lead to heightened functional connectivity of the same pathway (West et al., 2018).

Strengthening pallido-subthalamic inhibition was found to exponentially increase cortico-subthalamic synchronization. A weakening of the same pathway shifts coherence to higher frequency beta but has negligible effect upon the magnitude of the coherence. This suggests that at K < -0.7 (equivalent to ~50% of the fitted strength), the STN/GPe circuit does not play an active role in amplifying the low frequency components of the cortical rhythms but instead may act to feedforward higher frequency rhythms.

Different Feedback Loops Modulate Cortical and Subcortical Beta Activity and their Synchronization

Alterations of network state in the brain involve changes to multiple connections within the circuit, rather than just individual projections as has been looked at so far. In order to investigate the combined effect of different variations in connection strengths we simulated data from 500 models with random strengths drawn from the posterior distributions of the fitted model (see methods). We investigate five reciprocal loops thought to be important in maintenance of rhythmic activity (see figure 4A):

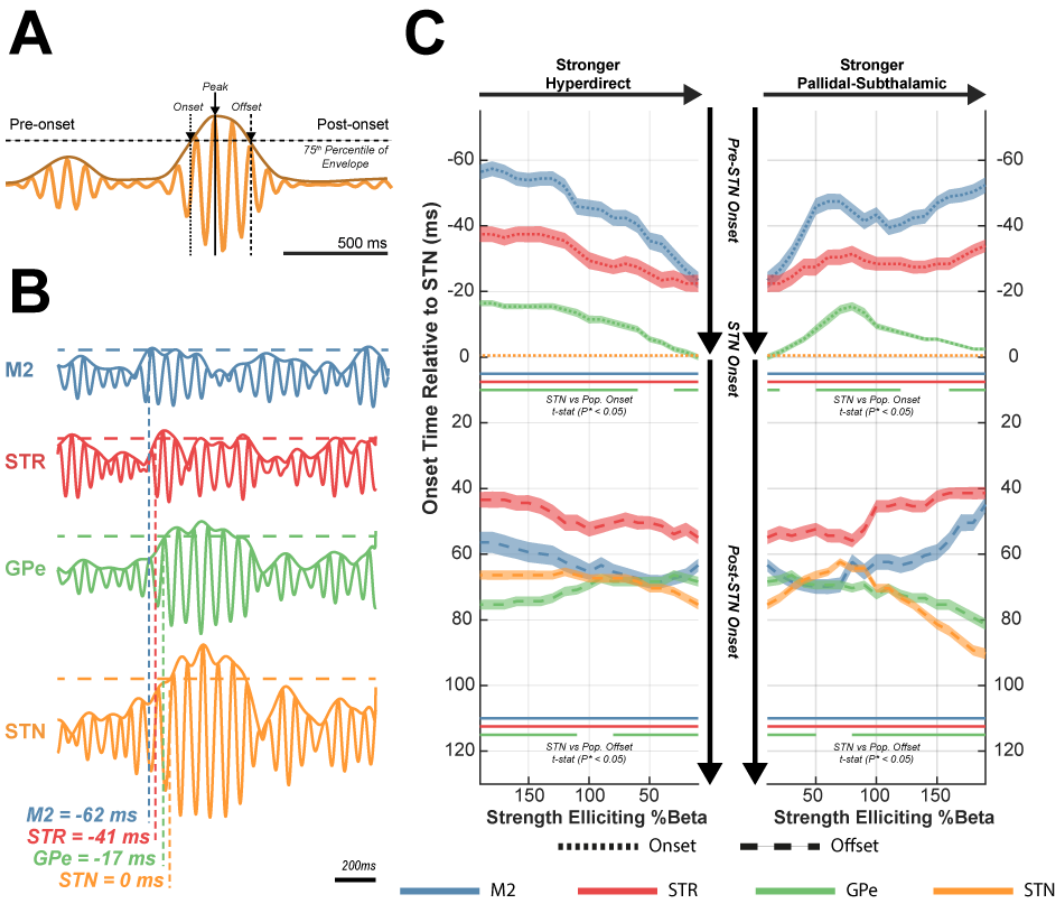

Figure 5 – **Time-locked analysis of simulated beta bursts across the cortico-basal-ganglia-thalamic circuit following modulation of STN inputs via excitatory hyperdirect (M2 → STN) projections and pallido-subthalamic inhibition (GPe → STN). (A)** Periods of high amplitude beta activity (burst events) were identified by thresholding the bandfiltered envelope at the 75th percentile of the data (per population and concatenated across all conditions). Bursts timings were estimated by the threshold crossing onset and offset. **(B)** Example 2s of simulated data shows the propagation of burst activity across the network, with the threshold crossings of each population annotated. All timings are set relative to the STN onset at t = 0 ms. **(C)** Ribbon diagram of the changes in burst timings following modulation of the hyperdirect (left panel) and pallido-subthalamic (right panel) connections. Colour coded lines for each node in the network are given to show the median burst onset (dotted) and offset (dashed) times with borders indicating the standard error of the median. Connection strengths are increased from left to right and are plot on a scale indicating the connection strength eliciting a

percentage change in beta power from that of the fitted model. Bold lines indicate simulations in which M2, STR, or GPe bursts onsets/offsets were significantly different from that in the STN (t-test, Bonferonni corrected $\alpha^* = \alpha/n$; where n = 18 separate tests).

1) direct: M2 → STR → GPi → Thal. → M2;
2) indirect: M2 → STR → GPe → STN → GPi → Thal. → M2;
3) hypedirect: M2 → STN → GPi → Thal. → STN;
4) thalamocortical: M2 → Thal. → M2;
5) pallido-subthalamic: GPe → STN → GPe.

The degree of connectivity within these loops is summarised using either the *net loop strength* (sum of the absolute connectivity strengths) or *net loop E/I balance* (sum of the signed connection strengths; see methods). The differences in these parameters between the models yielding STN beta power, M2 beta power, and STN/M2 coherence below or above the 1st or 4th quartile is presented in figure 4B.

Results in figure 4B show that for models yielding high STN beta power (1st column) there is an increased loop strength in both the pallido-subthalamic (-28.3 ±16.7, $t(33) = -6.9$, $P<0.001$, $\alpha^* = 003$) and indirect (-16.3 ±8.8, $t(33) = -7.5$, $P<0.001$, $\alpha^* = 0.003$) circuits. Correlation analysis of both pathways (supplementary information III and IV) also confirms the existence of strong linear relationship between the strengths of these pathways and the spectral features in question.

Importantly, different pathways modulate M2 beta power, with increased strength of the hyperdirect loop found to be critical (-22.1 ±19.3, $t(33) = -4.7$, $P = 0.001$, $\alpha^* = 003$) that is associated with an overall increase in loop excitation (-8.5 ±10.0, $t(33) = -3.5$, $P < 0.05$). It was found that the hyperdirect (-24.5 ±17.1, $t(33) = -5.8$, $P < 0.001$) and indirect pathways (-14.3 ±10.4, $t(33) = -5.6$, $P < 0.001$) increased in strength for models yielding large M2/STN coherences, again associated with an increased excitation. Correlation analysis of both pathways (supplementary information III and IV) confirms the existence of a strong linear relationship between pathway strength and the spectral features in question.

The Timing of Beta Burst Evolution Across the Network is Altered by Strength of Inputs to the STN

We next investigated how inputs to the STN alter the evolution of transient rhythmic activity in the beta frequency band (Tinkhauser et al., 2017b; Cagnan et al., 2019b) across the motor circuit. Beta burst propagation is demonstrated in three populations that lay upstream of the STN, while burst onset and offset are represented with respect to the emergence and termination of a beta burst at the STN, respectively. In figure 5B, an example set of narrowband (14-21 Hz) traces, simulated from the fitted

model, show a cascade of activity from M2 down indirect pathway to the STN, with timings that are summarised in figure 5C.

The sequence of beta burst emergence across the motor circuit is quantified in figure 5C which inspects the relationship of burst timing (time relative to the onset at the STN; plot on the y-axis) to connection strength (in terms of the related percentage change in beta power from the base model). In the fitted model (i.e. at 0% change), burst onsets occur sequentially: beginning at M2 at -45 ms; STR at -30 ms; and GPe at -15 ms prior to STN burst initiation at 0 ms. Strengthening pallido-subthalamic inhibition (5C, right panel) extends the period of suprathreshold activity in the STN/GPe by delaying their termination to 90 ms (compared to 70 ms in the base model) (*STN offset times for 100% vs 10% pallido-*

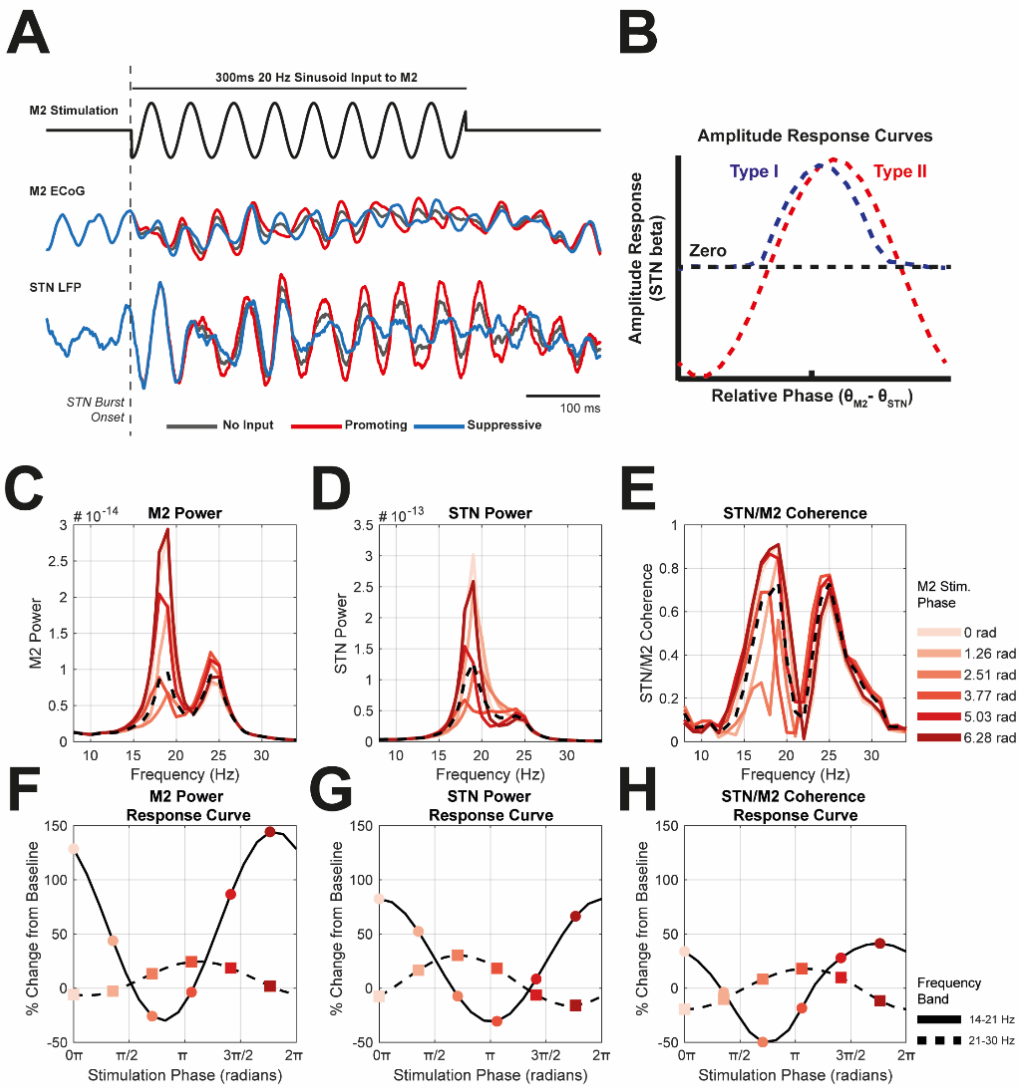

Figure 6 – Simulating closed loop stimulation of motor cortex when sensing bursts in the STN. Stimulation is phase locked to STN activity during high amplitude beta bursts. (A) Example simulation within a single STN burst: a high

amplitude STN burst was detected from simulations of the base model (onset indicated by grey dashed line, and time course shown by the bold grey line). Subsequent simulations used identical noise inputs to the network to ensure bursts were replicated. The timings of burst onsets were used to trigger a 300ms sinusoidal input to cortex (example shown in black; top) with its phase manipulated to have an offset with respect to that of ongoing beta activity in the STN. We show: In-phase to STN (red); and anti-phase to STN (blue) stimulation. (B) Schematic of an amplitude response curve (ARCs) used to characterize phase dependent effects of beta power. Curves can be non-phase dependent (constant), uniquely amplifying/suppressing (type I), or both (type II). (C, D, and E) Plots of M2 power spectra, STN power spectra, and STN/M2 coherence for six selected phase bins (indicated in legend). The dashed line gives the spectra from the unstimulated condition (i.e. base model). (F, G, H) Response curves corresponding to the spectra in the row above indicating the modulation of low beta (14-21 Hz; bold; circles) and high beta (21-30 Hz; dashed; squares) frequencies. Peaks are plot as a percentage difference from the base model (i.e unstimulated condition). Coloured symbols correspond to the sample phase bins of the spectra shown in the above row.

subthalamic strength: -17.4 ±2.7 ms, t(1671) = -12.74), whilst at the same time expediting suppression of activity at the M2 and STR by ~20 ms. These changes result in a divergence of corticostriatal and pallido-subthalamic termination times by > 50 ms. Additionally, increasing the strength of the GPe → STN connection broadens the effective window in which antecedent cortical fluctuations may cascade to form a burst in STN/GPe subcircuit, with cortical bursts occurring > -55 ms prior to that seen in the STN (compared with -40 ms in the base model).

In contrast, strengthening of the hyperdirect pathway (5C, left panel) brings cortico-striatal activities closer in time to that of the STN. At strengths eliciting less than 60% power of beta from the fitted model, the onset of bursts in M2 is sufficiently slowed (*M2 onset times for 100% vs 10% hyperdirect strength*,: 9 ±7.0 ms, t(553) = -2.75) such that they coincide very closely with activity initiated in the STR. In all the cases simulated, striatal bursts terminate before that in M2 suggesting they require cortical drive in order to be sustained. Overall, cortico-subthalamic connectivity compresses the timings of burst termination for all four regions analysed such that bursts are extinguished within a window of 30 ms, in the strongest case tested.

Pathway Strength Dictates the Probability of Burst Coincidence Across the Network

To examine how bursts cooccurred we not only test for their relative timing, but also the rate of coincidence. For example, bursts in the cortex usually precedes that in the STN, what is likelihood that burst will result in an STN burst? This analysis is presented in the figure shown in supplementary information VI. These results show that in general bursts are highly synchronous across the network with the majority of analyses showing >70% chance of bursts coinciding with the reference burst within a 300ms window either side of its onset. Importantly, these results show that the choice of site at which the reference burst is defined is important in determining the probability of whether a burst will cooccur at another site.

Results indicate that if the pallidal-subthalamic pathway is weak (i.e. 50% strength of that in the base model), the probability of a cortical burst triggering a coincident burst in the STN/GPe complex is

<40%, increasing up to >80% at large strengths (150% strength of that in the base model). If we look vice versa, switching the reference to the STN, we show that when the pathway is weak >95% of GPe bursts coincide with that in the cortex. Interestingly, strengthening the pallidal input acts to reduce the dependence of GPe burst emergence upon antecedent cortical bursts (<75 coincidence). These results add further weight to the idea that the STN/GPe complex enters into an autonomously oscillating state with increased pallidal inhibition.

Phase Locked Stimulation of Motor Cortex Triggered by Beta Bursts in the Subthalamic Nucleus

The previous analyses show that for all models examined, inputs from the cortex form an important influence on determining the evolution of beta power across the motor circuit. In the next set of simulations, the importance of the timing of cortical activity in terms of the regulation of STN beta bursts was probed by modulating cortical phase. Figure 6A demonstrates that STN beta activity can be either amplified or suppressed dependent upon relative phase of modulated cortical activity. When close to anti-phase, there is an enhancement of STN beta, and a suppression when in-phase. These

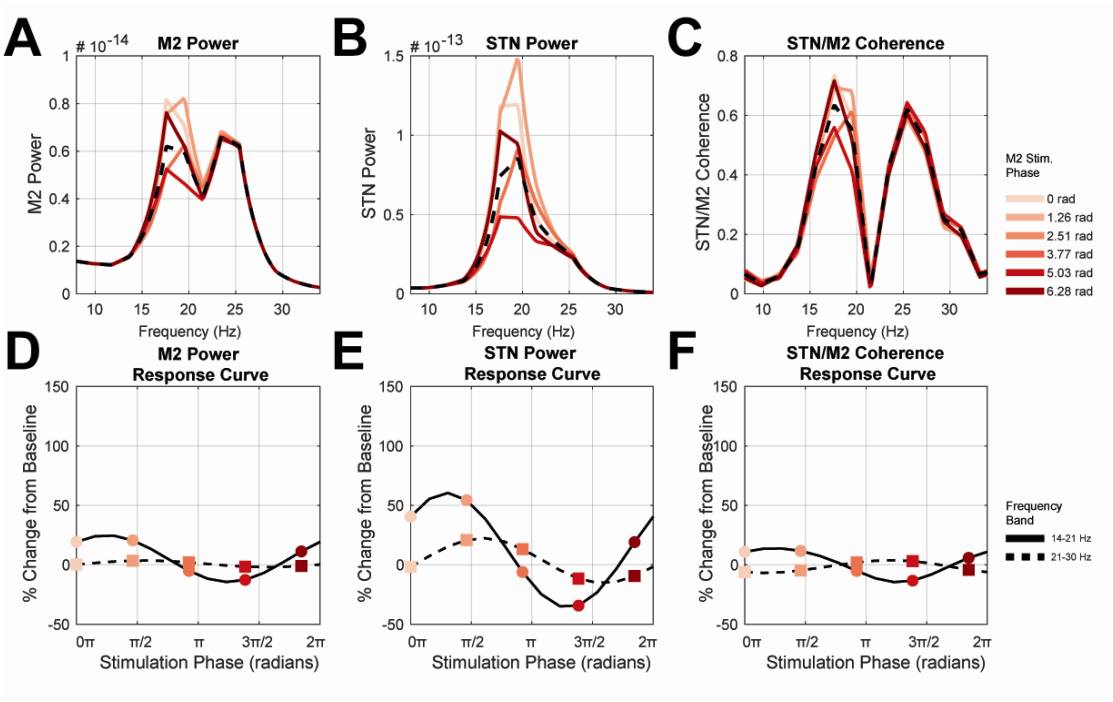

effects presumably occur due to constructive/destructive interference, with the precise phase of the effect matched to the propagation delays involved in predominant route of propagation. These effects impact the spectra of both the motor cortex (figure 6C) and STN (figure 6D), as well as their coherence (figure 6E).

Figure 7 – **Simulating closed loop stimulation of STN when sensing bursts in the motor cortex. Stimulation is phase locked to cortical activity during high amplitude beta bursts. (A, B, and C)** Plots of M2 power spectra, STN power spectra, and STN/M2 coherence for six selected phase bins (given in legend). The dashed line gives the spectra from the unstimulated condition (i.e. base model). **(D, E, F)** Response curves corresponding to the spectra in the row above indicating the modulation of low beta (14-21 Hz; bold; circles) and high beta (21-30 Hz; dashed; squares) frequencies. Peaks are plot as a percentage difference from the base model. Coloured symbols correspond to the sample phase bins of the spectra shown in the above row.

The phase specific effects of stimulation can be characterised by constructing an amplitude response curve (ARC; figure 6B). When sweeping cortical stimulation over a large range of phases (0π to 2π rads in 18 bins) there is a significant modulation of the power spectra of the STN (figure 6B). At amplifying phases of input, low frequency beta (14-21 Hz) is selectively enhanced; whilst at suppressing phase, higher frequency beta (21-30 Hz) is accentuated. This effect can be seen in more detail in figure 6C where the amplitude response curves of the two frequency peaks are summarised. These results indicate that the range of phases in which it is possible to achieve a suppressive effect (5/18 phase bins tested with a maximum reduction of 32%) is smaller than that found to be amplifying of beta (13/18 of phases simulated with a maximum amplification of 72%). The differential effect on low and high beta frequencies was found to be near antiphase in their relationship.

Phase Locked Stimulation of STN Triggered by Beta Bursts in the Motor Cortex

The results presented in the section *Pathway Strength Dictates the Probability of Burst Coincidence Across the Network* suggests that there is a high coincidence between upstream cortical beta bursts and that measured in the STN. In this section of results we present simulations of phase locked stimulation of the STN triggered by cortical beta bursts. In figure 7, it can be seen that the effects of stimulation of STN are different to that when modulating cortical activity, namely the location specificity is greater as there far less modulation of cortical activity (figure 7A vs figure 6C). Furthermore modulation of cortico-subthalamic coherence is also negligible providing < 15% change from the baseline (figure 7C).

Phase Locked Stimulation of Cortex can Modulate Properties of Burst Activity in the Subthalamic Nucleus

We next investigate precisely how phasic stimulation modulates rhythmic activity in the circuit by making an analysis of the effects upon the temporal properties of beta activity (supplementary information VII). We show that stimulation of the motor cortex at beta suppressive phases acts predominantly through the abridgment of burst durations (*suppressive stim. vs base.;* 19.2 ± 13.5 ms, $t(302) = 2.8$, $P = 0.005$, $\alpha^* = 0.01$) rather than through reduction in amplitude (*suppressive stim. vs base.;* $3 \times 10^{-8} \pm 4 \times 10^{-8}$, $t(302) = 1.5$, $P = 0.124$, $\alpha^* = 0.01$). Suppressive stimulation also reduces the burst rate (*suppressive stim. vs base.* difference of -10 min^{-1}). These effects accompany an overall reduction of within burst cortico-subthalamic synchrony (*suppressive stim. vs base.;* -0.15 ± 0.10, $t(302) = 6.22$, $P < 0.001$, $\alpha^* = 0.01$).

Modulation of STN Beta Amplitude by Cortico-Subthalamic Relative Phase is State Dependent

In figure 8, the effect of modulating the strength of inputs to the STN upon the efficacy of phasic stimulation of the motor cortex is examined. These analyses show that the profiles of the ARCs are significantly altered by changes in connectivity (examples shown in figure 8A and D). These changes involve both changes in the maximum suppression or amplification, as well as shifts in their respective phases. The dependency of ARC properties upon GPe → STN connectivity is shown in figure 8B. Response profiles when this connection is weak (less than 100% strength) are type II, although amplification is always larger than the corresponding suppression. Analysis of the maximal suppressive/amplifying phase (figure 8C) indicates a clear transition around 75% base connectivity strength. This result arises from a shift in pathways responsible for the maintenance of beta oscillations where above 75% strength suppressive phases must focus upon disturbing STN/GPe resonance rather than feedforward propagation of cortical rhythms.

Modulation of the hyperdirect pathway shows that this pathway has less impact on the efficacy of cortical stimulation in reducing STN beta rhythms: in figure 8D there is a clear shift in the effective phase of stimulation (with a transition occurring around 125% of the base strength; figure 8F). In all cases amplification fell within the range of 40-75% increase, versus a -40% to -10% suppression (figure 8E). Again, the clear switch in phase (figure 8F) indicates a transition in propagation, likely due to hyperdirect transmission predominating over that going through the indirect axis at large connection strengths.

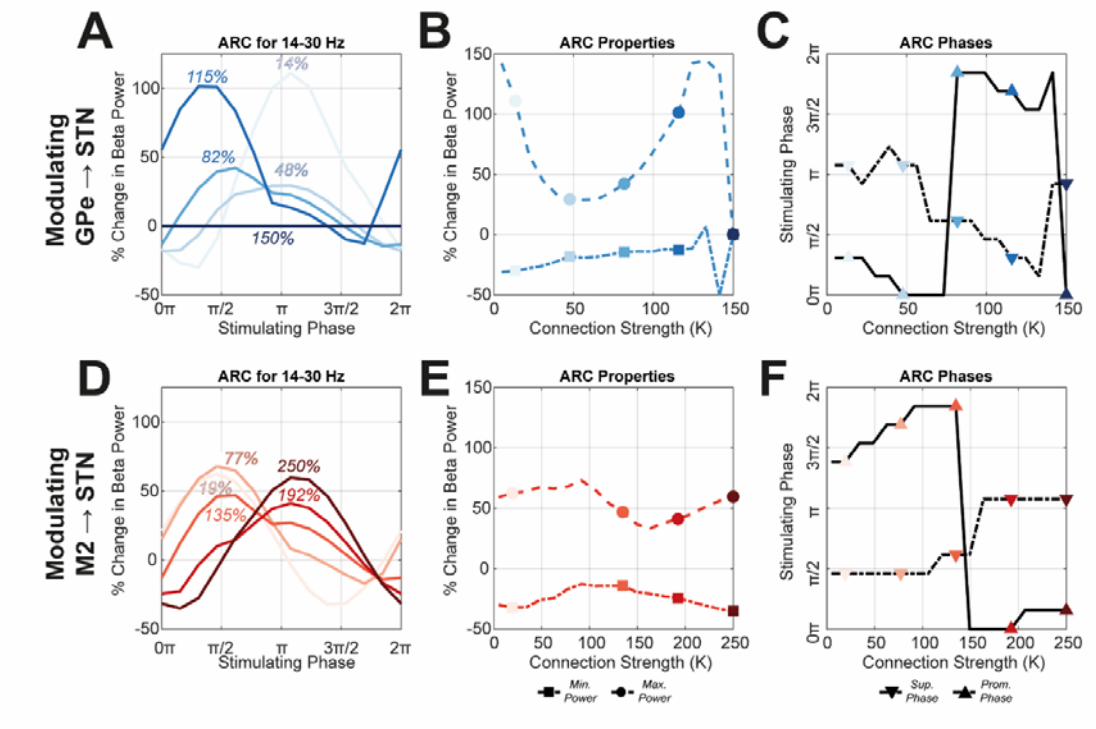

Figure 8 – **Simulating state dependent changes in the efficacy of phase specific stimulation of motor cortex (M2) when modulating the strength of the pallido-subthalamic (GPe → STN) and hyperdirect (M2 → STN) connections. (A)** Simulated ARCs when the strength of the GPe → STN connection is altered from 14% to 150% with respect to the base model. These ARCs exhibit changes in maximum suppression/amplification, as well as shifts in phase. Changes in power are scaled as the percentage difference from the unstimulated for each connection strength. **(B)** The ARCs were characterised by taking the minimum (dotted line; circles) and maximum (dashed line; squares) power and then plotting these against the corresponding connection strength. The coloured markers correspond to the samples shown in (A). **(C)** Plot of the maximum suppressive (dashed; downwards arrows) and promoting (bold; upwards arrows) versus connection strength. There is a clear transition in phase close to 75% connection strength. **(D, E, F)** Same as (A, B, C) but for simulations modulating the M2 → STN connection.

Discussion

Summary of Findings

We have shown that the emergence and timing of beta oscillations in the STN, a common biomarker of the motor deficits associated with Parkinsonism, are under the influence of an interplay of parallel loops within the cortico-basal ganglia-thalamic circuit. The convergence of inhibitory and excitatory inputs from the external pallidum and motor cortex respectively at the STN, makes the balance of loops involving these pathways vital determinants of the properties and timing of intermittent beta rhythms propagating across this circuit. Further, our simulations demonstrate that cortical beta rhythms are under influence of distinct circuits, separated in frequency from those preferentially propagated by the STN/GPe couplet. These results also provide explanation for paradoxical findings

that dopamine depletion can result in enhanced cortical-subthalamic synchronization (Sharott et al., 2005; West et al., 2018; Baaske et al., 2019)during synaptic weakening of glutamatergic inputs to the STN (Mathai et al., 2015b; Chu et al., 2017). Simulations of activity in this pathway demonstrate a non-monotonic relationship between cortico-subthalamic effective connectivity and its resulting synchronization. Finally, we have shown how changes in network state can significantly alter the amplitude response of STN beta rhythms in reaction to phase locked inputs arriving from the motor cortex. These results help build a better understanding of the technical challenges that will need to be overcome in order to achieve neuromodulation that is adaptive to spontaneous changes in brain state.

The Amplitude of STN Beta Rhythms is Highly Influenced by Alterations in Network Connectivity

At their most basic, strategies for therapeutic brain stimulation, such as cDBS for PD provide stimulation using static parameters (i.e. frequency and amplitude), chosen to provide clinically significant reductions in symptom expression whilst minimising undesired adverse effects (Castrioto et al., 2014; Cagnan et al., 2019a). Strategies for state of the art neuromodulation now aim to identify a biomarker associated with a pathological or functional state, and then use this signal as a control signal to gate the delivery of stimulation (Bouthour et al., 2019).

In this paper we describe how the differential expression of STN beta, a key biomarker being used for delivery of therapeutic DBS for PD, results from shifts in the engagement of different pathways of the cortico-basal ganglia-thalamic circuit. A prevailing view strongly implicates the engagement of the STN/GPe loop in pathological brain states associated with aberrant STN beta amplitude (Mallet et al., 2008a; Cruz et al., 2011; Tachibana et al., 2011). The results presented here indicate that the propensity of this subcircuit to enter into a resonant state arises from an interplay of hyperdirect and pallidal inputs impinging upon the STN. This matches well with previous models (Pavlides et al., 2015; Fountas and Shanahan, 2017) that propose that the STN/GPe loop selectively resonates at beta frequency to inputs arriving from the motor cortex, as well as experimental findings that Parkinsonism predisposes the circuit to synchronization by the cortex (Baaske et al., 2019). Furthermore, recent experimental work demonstrates that high frequency stimulation of the STN acts to shift the relative timing of excitatory and inhibitory inputs to the STN (Amadeus Steiner et al., 2019) to hinder entrainment of the STN/GPe circuit (Moran et al., 2012). In contrast to previous work (van Albada et al., 2009; Brazhnik et al., 2016; Reis et al., 2019) we find little evidence that the corticothalamic relay (acting in insolation from basal ganglia output) reinforces STN low beta rhythms, but may instead support the maintenance of higher frequency beta rhythms in the cortex (Sherman et al., 2016). This work agrees with the principle of competing loops introduced by Leblois et al. (2006) but differs in that the hyperdirect pathway in this model seems to act in antagonism with that of the indirect, rather than direct. We also provide evidence for a segregation of low and high frequency beta between indirect and hyperdirect loops with findings supporting a role for the thalamocortical relay in the

propagation of higher frequency beta activity such as that observed in the cortex during movement (Brazhnik et al., 2016), such as that reported by Brazhnik et al., (2016). It is however important to note that this study did not use thalamic recordings to constrain model parameters, which may explain its relative unimportant role in the presented model.

Disrupting Antecedent Cortical Activity May Provide Selective Targeting of Pathological Activity

Simulations of the model in this paper demonstrate that beta activity evolves as it propagates throughout the different loops of the circuit. In all simulations, high amplitude bursts in basal ganglia were preceded by that in the cortex, a finding in agreement with a wide body of experimental evidence (Williams et al., 2002; Fogelson et al., 2006; Lalo et al., 2008; Litvak et al., 2011; Sharott et al., 2018). Analysis of the timing of the initiation and termination of beta burst activity in the model demonstrates how the increased receipt of pallidal inputs to the STN can result in burst elongation which can explain recently reported findings that pathological activity can be preferentially identified by long beta bursts (Deffains et al. 2018; Tinkhauser et al. 2018). A synthesis of the two above findings suggest that whilst pathological activity may begin with cortical activity, it is subverted by its transformation at the STN/GPe loop (Cagnan et al., 2019b), which given sufficient strength of feedback from the pallidum and coherent phase alignment with cortex, will resonate at lower beta frequencies (< 21 Hz). Given significant pallidal inhibition, resonant dampening of the STN/GPe loop is sufficiently weakened to give rise to autonomous subcortical oscillations that terminate several cycles later from that of cortical activity. This predicts that experimentally recorded bursts in the cortex and STN should diverge in lengths with increased excitation of the GPe. More importantly, it suggests that interruption of precursor activity in the cortex may be used to extinguish conditions that pre-empt emergence of pathological resonance in the cortex without disrupting normal functional activity.

The Responses of STN Beta Rhythm to Phase Specific Neuromodulation are State Dependent

Rather than triggering stimulation according to changes in a given biomarker such as STN beta, phasic stimulation delivers precisely timed stimulation to interact with activity of an oscillating control signal. This approach follows on from the fact that neuronal ensembles demonstrate phase locked firing to population activity and so precisely timed stimulation relative to the preferential phase may act to modulate brain rhythms themselves via constructive or destructive interference (Rosenblum and Pikovsky, 2004; Holt et al., 2016). This approach has been demonstrated to be effective in modulating tremor (Brittain et al., 2013; Cagnan et al., 2017), as well as supressing beta oscillations in both Parkinsonian patients (Holt et al., 2019), and in healthy (Peles et al., 2019) and MTPT primates (Sanabria et al., 2020). In the simulations presented here we demonstrate how phase locking of cortical stimulation to STN beta rhythms can act to selectively enhance or suppress oscillatory activity as well as its interregional synchronization.

A systems level understanding of the mechanisms of deep brain stimulation can enhance the targeting of pathways to block the propagation of pathological neuronal activity whilst leaving functional networks intact (McIntyre and Hahn, 2010). However, brain networks are highly dynamic and undulate with changes in many factors such as task demand, arousal states, and diurnal rhythms (Raichle, 2011; Lee and Dan, 2012). This suggests that the parameters required for optimal therapeutic neuromodulation are likely to be context dependent (Bergmann et al., 2016; Karabanov et al., 2016).

In this work we have demonstrated that the phase specific response of STN beta to stimulation will be differentially effective dependent upon inhibitory drive from the GPe, which is itself largely under influence from spiny projection neurons originating in the striatum and under modulation by tonic changes in dopamine (Gillies et al., 2002; Kumar et al., 2011; Sharott et al., 2017). Across the simulations shown here we show that it is possible to elicit both non-phasic, exclusively amplifying, as well as both amplifying and suppressive amplitude response curves, dependent upon the exact strength of the pallido-subthalamic pathway. The relationship between the phase dependent effects and connectivity are highly nonlinear even when modulating a single connection. Recent computational work suggests that the efficacy of phase locked stimulation is likely to be dependent upon the amplitude of activity (Tass, 2000; Weerasinghe et al., 2019). This would suggest that static approaches to selecting stimulation control parameters are likely to face difficulties in the face of spontaneous changes in brain state such as those associated with movement. Future stimulation strategies that can provide dynamic parameterization of stimulation may adopt state estimation techniques (Baker et al., 2014); or dual control algorithms that provide therapeutic stimulation at the same time as actively exploring stimulations parameters in order to optimize therapeutic benefits (Grado et al., 2018).

Targeting Interareal Synchronization with Phase Locked Stimulation to Compensate Structural Degeneration

The presented simulation study has unveiled different pathways involved in the promotion of beta rhythms in the cortex and STN suggesting a functional distinction between the two. Results show that lower frequency rhythms at the STN are predominantly under the influence of the indirect loop, whilst beta power in the motor cortex (and its synchronization with the STN) is better explained by enhancement of the hyperdirect loop. Experimental evidence has shown that dopamine depletion reinforces pallidal inhibition (Fan et al., 2012; Chu et al., 2015), whilst at the same time reducing hyperdirect enervation of the STN (Mathai et al., 2015a; Chu et al., 2017; Wang et al., 2018). Cortical and subcortical beta rhythms show considerable variation, for instance shifting to higher frequencies during movement (Brazhnik et al., 2014), suggesting their expression is the product of rebalancing of loop activity.

Our simulations demonstrate that at phases of stimulation maximally supressing low frequency beta rhythms, there is a simultaneous enhancement of higher frequencies (>21 Hz). Interestingly, this effect mimicked results of simulations in which the hyperdirect pathway was enhanced by acting to increase cortico-subthalamic coupling at the higher frequency range. Similar results have been demonstrated experimentally (Sanabria et al., 2020) where an higher frequency beta rhythms (>18 Hz) emerged during phasic DBS targeted to 11-17 Hz rhythms. These results suggest that phasic suppression of pathological activity in arising in the indirect pathway may be able to shift global activity in favour of propagation via other loop. The potential ability to rebias activity in this circuit is likely to have important implications for motor execution and planning (Frank et al., 2007; Jahfari et al., 2011). On the other hand, these data suggest that stimulation at sub-optimal phases can act to "push" pathological activity to lower or higher sidebands without achieving a complete suppression of the target rhythm- a phenomena that has been previously observed in phase locked stimulation for tremor (Cagnan et al., 2017). Simulations within this paper suggest that these effects can be controlled by careful determination of both the "sensing" site at which pathological activity is detected, as well as the site at which stimuli are delivered.

Translating Phase Locked Stimulation to Non-Parkinsonian Disorders and Non-Therapeutic Neurostimulation

High frequency cDBS is a highly effective for treatment for many of the motor deficits associated with Parkinsonism, and the reduction in adverse effects and increased power efficiency remain important goals. However, novel neuromodulation strategies such as that introduced here, are likely to be fruitful in other contexts involving neural mechanisms that can be leveraged by the highly precise stimulation that these technique afford. Numerous neurodegenerative disorders (Llinás et al., 1999; Schnitzler and Gross, 2005; Tye and Deisseroth, 2012), as well as mechanisms of functional brain activity (Varela et al., 2001; Bressler and Menon, 2010; Thut et al., 2012) have been related to altered interareal neural synchronization that could be potentially modulated by multisite sensing/stimulation. For instance, the high temporally patterned structure of cortico-hippocampal activity involved in memory (Sirota et al., 2008) has made this system well suited to the use of theta frequency-locked stimulation (Reinhart and Nguyen, 2019) to modulate memory. From this it is likely that techniques developed within well studied circuits such as the cortico-basal ganglia network will find translation to other important functional networks in the brain.

Conclusions

This study builds upon our understanding of the emergence of beta oscillations in the cortical-basal ganglia circuit from activity propagating within the multiple loops formed by this network. Our results suggest that heightened beta activity in the STN results from the strengthening of the indirect axis, whilst beta activity in the motor cortex is promoted by the hyperdirect loop and its thalmocortical return. Analysis of the state dependent changes in burst timings suggest that strengthening of pallidal

input to the STN leads to the emergence of autonomy of beta rhythms in the STN/GPe circuit independent of cortical input. Finally, we show that subcortical beta rhythms can be modulated by precisely timed stimulation of the cortex with a response that is non-trivially related to network connectivity. These results support novel approaches to neuromodulation that can adapt stimulation in accordance with changes in brain state.

References

Amadeus Steiner L, Barreda Tomás FJ, Planert H, Alle H, Vida I, Geiger JRP (2019) Connectivity and dynamics underlying synaptic control of the subthalamic nucleus. J Neurosci 39:2470–2481.

Arlotti M, Rosa M, Marceglia S, Barbieri S, Priori A (2016) The adaptive deep brain stimulation challenge. Parkinsonism Relat Disord 28:12–17 Available at: https://www.sciencedirect.com/science/article/abs/pii/S1353802016300748 [Accessed July 17, 2019].

Baaske MK, Kormann E, Holt AB, Gulberti A, McNamara CG, Pötter-Nerger M, Westphal M, Engel AK, Hamel W, Brown P, Moll CKE, Sharott A (2019) Parkinson's disease uncovers an underlying sensitivity of subthalamic nucleus neurons to beta-frequency cortical input. bioRxiv:513234 Available at: https://www.biorxiv.org/content/10.1101/513234v3 [Accessed February 20, 2020].

Baker AP, Brookes MJ, Rezek IA, Smith SM, Behrens T, Probert Smith PJ, Woolrich M (2014) Fast transient networks in spontaneous human brain activity. Elife 3 Available at: http://www.ncbi.nlm.nih.gov/pmc/articles/PMC3965210/ [Accessed September 30, 2015].

Beaumont MA, Zhang W, Balding DJ (2002) Approximate Bayesian Computation in Population Genetics. Genetics 162:2025 LP – 2035 Available at: http://www.genetics.org/content/162/4/2025.abstract.

Bergmann TO, Karabanov A, Hartwigsen G, Thielscher A, Siebner HR (2016) Combining non-invasive transcranial brain stimulation with neuroimaging and electrophysiology: Current approaches and future perspectives. Neuroimage 140:4–19.

Bevan MD, Magill PJ, Terman D, Bolam JP, Wilson CJ (2002) Move to the rhythm: oscillations in the subthalamic nucleus–external globus pallidus network. Trends Neurosci 25:525–531.

Bhatt MB, Bowen S, Rossiter HE, Dupont-Hadwen J, Moran RJ, Friston KJ, Ward NS (2016) Computational modelling of movement-related beta-oscillatory dynamics in human motor cortex. Neuroimage 133:224–232 Available at: http://dx.doi.org/10.1016/j.neuroimage.2016.02.078.

Bouthour W, Mégevand P, Donoghue J, Lüscher C, Birbaumer N, Krack P (2019) Biomarkers for closed-loop deep brain stimulation in Parkinson disease and beyond. Nat Rev Neurol 15:343–352.

Brazhnik E, McCoy AJ, Novikov N, Hatch CE, Walters JR (2016) Ventral medial thalamic nucleus promotes synchronization of increased high beta oscillatory activity in the basal ganglia-thalamocortical network of the hemiparkinsonian rat. J Neurosci 36:4196–4208.

Brazhnik E, Novikov N, McCoy AJ, Cruz A V, Walters JR (2014) Functional correlates of exaggerated oscillatory activity in basal ganglia output in hemiparkinsonian rats. Exp Neurol 261:563–577 Available at: https://pubmed.ncbi.nlm.nih.gov/25084518.

Bressler SL, Menon V (2010) Large-scale brain networks in cognition: emerging methods and principles. Trends Cogn Sci 14:277–290.

Brittain J-S, Brown P (2014) Oscillations and the basal ganglia: motor control and beyond. Neuroimage 85:637–647.

Brittain JS, Probert-Smith P, Aziz TZ, Brown P (2013) Tremor suppression by rhythmic transcranial current stimulation. Curr Biol 23:436–440.

Brown P (2007) Abnormal oscillatory synchronisation in the motor system leads to impaired movement. Curr Opin Neurobiol 17:656–664.

Brown P, Oliviero A, Mazzone P, Insola A, Tonali P, Di Lazzaro V (2001) Dopamine Dependency of Oscillations between Subthalamic Nucleus and Pallidum in Parkinson's Disease. J Neurosci 21:1033–1038 Available at: http://www.jneurosci.org/content/21/3/1033.abstract [Accessed January 4, 2016].

Cagnan H, Denison T, McIntyre C, Brown P (2019a) Emerging technologies for improved deep brain stimulation. Nat Biotechnol 37:1024–1033.

Cagnan H, Duff EP, Brown P (2015) The relative phases of basal ganglia activities dynamically shape effective connectivity in Parkinson's disease. Brain 138:1667–1678 Available at: http://brain.oxfordjournals.org/content/138/6/1667 [Accessed October 1, 2015].

Cagnan H, Mallet N, Moll CKE, Gulberti A, Holt AB, Westphal M, Gerloff C, Engel AK, Hamel W, Magill PJ, Brown P, Sharott A (2019b) Temporal evolution of beta bursts in the parkinsonian cortical and basal ganglia network. Proc Natl Acad Sci U S A:201819975 Available at: http://www.ncbi.nlm.nih.gov/pubmed/31341079 [Accessed July 29, 2019].

Cagnan H, Pedrosa D, Little S, Pogosyan A, Cheeran B, Aziz T, Green A, Fitzgerald J, Foltynie T, Limousin P, Zrinzo L, Hariz M, Friston KJ, Denison T, Brown P (2017) Stimulating at the right

time: phase-specific deep brain stimulation. Brain 140:132–145 Available at: https://academic.oup.com/brain/article-lookup/doi/10.1093/brain/aww286 [Accessed June 15, 2018].

Castrioto A, Lhommée E, Moro E, Krack P (2014) Mood and behavioural effects of subthalamic stimulation in Parkinson's disease. Lancet Neurol 13:287–305.

Chu H-Y, Atherton JF, Wokosin D, Surmeier DJ, Bevan MD (2015) Heterosynaptic Regulation of External Globus Pallidus Inputs to the Subthalamic Nucleus by the Motor Cortex. Neuron 85:364–376 Available at: https://www.sciencedirect.com/science/article/pii/S0896627314011039 [Accessed July 17, 2019].

Chu HY, McIver EL, Kovaleski RF, Atherton JF, Bevan MD (2017) Loss of Hyperdirect Pathway Cortico-Subthalamic Inputs Following Degeneration of Midbrain Dopamine Neurons. Neuron 95:1306-1318.e5 Available at: https://doi.org/10.1016/j.neuron.2017.08.038.

Cordon I, Nicolás MJ, Arrieta S, Alegre M, Artieda J, Valencia M (2018) Theta-phase closed-loop stimulation induces motor paradoxical responses in the rat model of Parkinson disease. Brain Stimul 11:231–238 Available at: https://www.sciencedirect.com/science/article/pii/S1935861X1730935X [Accessed December 2, 2019].

Cruz A V., Mallet N, Magill PJ, Brown P, Averbeck BB (2011) Effects of dopamine depletion on information flow between the subthalamic nucleus and external globus pallidus. 106:2012–2023.

David O, Friston KJ (2003) A neural mass model for MEG/EEG: Neuroimage 20:1743–1755 Available at: http://www.sciencedirect.com/science/article/pii/S1053811903004579 [Accessed February 2, 2016].

de Solages C, Hill BC, Koop MM, Henderson JM, Bronte-Stewart H (2010) Bilateral symmetry and coherence of subthalamic nuclei beta band activity in Parkinson's disease. Exp Neurol 221:260–266 Available at: http://www.sciencedirect.com/science/article/pii/S0014488609004701 [Accessed March 30, 2016].

Deffains M, Iskhakova L, Katabi S, Haber SN, Israel Z, Bergman H (2016) Subthalamic, not striatal, activity correlates with basal ganglia downstream activity in normal and parkinsonian monkeys. Elife 5:1–38.

Deffains M, Iskhakova L, Katabi S, Israel Z, Bergman H (2018) Longer β oscillatory episodes reliably identify pathological subthalamic activity in Parkinsonism. Mov Disord 33:1609–1618.

Delaville C, Cruz A V, McCoy AJ, Brazhnik E, Avila I, Novikov N, Walters JR (2014) Oscillatory Activity in Basal Ganglia and Motor Cortex in an Awake Behaving Rodent Model of Parkinson's Disease. Basal Ganglia 3:221–227 Available at: http://www.ncbi.nlm.nih.gov/pubmed/25667820 [Accessed August 24, 2017].

Dostrovsky J, Bergman H (2004) Oscillatory activity in the basal ganglia--relationship to normal physiology and pathophysiology. Brain 127:721–722 Available at: https://academic.oup.com/brain/article-lookup/doi/10.1093/brain/awh164 [Accessed February 10, 2017].

Engel AK, Fries P (2010) Beta-band oscillations—signalling the status quo? Curr Opin Neurobiol 20:156–165.

Fan KY, Baufreton J, Surmeier DJ, Chan CS, Bevan MD (2012) Proliferation of External Globus Pallidus-Subthalamic Nucleus Synapses following Degeneration of Midbrain Dopamine Neurons. J Neurosci 32:13718–13728 Available at: https://www.jneurosci.org/content/32/40/13718.long [Accessed July 17, 2019].

Feingold J, Gibson DJ, DePasquale B, Graybiel AM (2015) Bursts of beta oscillation differentiate postperformance activity in the striatum and motor cortex of monkeys performing movement tasks. Proc Natl Acad Sci 112:13687–13692 Available at: http://www.pnas.org/lookup/doi/10.1073/pnas.1517629112.

Fogelson N, Williams D, Tijssen M, van Bruggen G, Speelman H, Brown P (2006) Different Functional Loops between Cerebral Cortex and the Subthalmic Area in Parkinson's Disease. Cereb Cortex 16:64–75 Available at: http://academic.oup.com/cercor/article/16/1/64/341423/Different-Functional-Loops-between-Cerebral-Cortex [Accessed July 17, 2019].

Fountas Z, Shanahan M (2017) The role of cortical oscillations in a spiking neural network model of the basal ganglia. PLoS One 12:e0189109.

Frank MJ, Samanta J, Moustafa AA, Sherman SJ (2007) Hold your horses: impulsivity, deep brain stimulation, and medication in parkinsonism. Science 318:1309–1312 Available at: http://www.sciencemag.org/content/318/5854/1309.long [Accessed January 4, 2016].

Fries P (2015) Rhythms for Cognition: Communication through Coherence. Neuron 88:220–235 Available at: http://www.sciencedirect.com/science/article/pii/S0896627315008235 [Accessed October 8, 2015].

Gillies A, Willshaw D (2004) Models of the subthalamic nucleus: The importance of intranuclear connectivity. Med Eng Phys 26:723–732.

Gillies, Willshaw D, Li Z (2002) Subthalamic-pallidal interactions are critical in determining normal and abnormal functioning of the basal ganglia. Proc R Soc B Biol Sci 269:545–551.

Grado LL, Johnson MD, Netoff TI (2018) Bayesian adaptive dual control of deep brain stimulation in a computational model of Parkinson's disease Santaniello S, ed. PLOS Comput Biol 14:e1006606 Available at: http://dx.plos.org/10.1371/journal.pcbi.1006606 [Accessed February 19, 2020].

Halliday DM, Senik MH, Stevenson CW, Mason R (2016) Non-parametric directionality analysis – Extension for removal of a single common predictor and application to time series. J Neurosci Methods 268:87–97 Available at: http://www.sciencedirect.com/science/article/pii/S0165027016300863 [Accessed April 25, 2017].

Hammond C, Bergman H, Brown P (2007) Pathological synchronization in Parkinson's disease: networks, models and treatments. Trends Neurosci 30:357–364 Available at: http://www.sciencedirect.com/science/article/pii/S0166223607001233 [Accessed October 20, 2015].

Haynes WIA, Haber SN (2013) The Organization of Prefrontal-Subthalamic Inputs in Primates Provides an Anatomical Substrate for Both Functional Specificity and Integration: Implications for Basal Ganglia Models and Deep Brain Stimulation. J Neurosci 33:4804–4814 Available at: https://www.jneurosci.org/content/33/11/4804.

Herz DM, Little S, Pedrosa DJ, Tinkhauser G, Cheeran B, Foltynie T, Bogacz R, Brown P (2018) Mechanisms Underlying Decision-Making as Revealed by Deep-Brain Stimulation in Patients with Parkinson's Disease. Curr Biol 28:1169-1178.e6 Available at: https://www.sciencedirect.com/science/article/pii/S0960982218302422?via%3Dihub [Accessed April 26, 2018].

Holt AB, Kormann E, Gulberti A, Pötter-Nerger M, McNamara CG, Cagnan H, Baaske MK, Little S, Köppen JA, Buhmann C, Westphal M, Gerloff C, Engel AK, Brown P, Hamel W, Moll CKE, Sharott A (2019) Phase-Dependent Suppression of Beta Oscillations in Parkinson's Disease Patients. J Neurosci 39:1119–1134 Available at: https://www.jneurosci.org/content/39/6/1119 [Accessed December 13, 2019].

Holt AB, Wilson D, Shinn M, Moehlis J, Netoff TI (2016) Phasic Burst Stimulation: A Closed-Loop Approach to Tuning Deep Brain Stimulation Parameters for Parkinson's Disease Sporns O, ed. PLOS Comput Biol 12:e1005011 Available at: http://dx.plos.org/10.1371/journal.pcbi.1005011 [Accessed November 24, 2016].

Jahfari S, Waldorp L, van den Wildenberg WPM, Scholte HS, Ridderinkhof KR, Forstmann BU (2011) Effective Connectivity Reveals Important Roles for Both the Hyperdirect (Fronto-Subthalamic) and the Indirect (Fronto-Striatal-Pallidal) Fronto-Basal Ganglia Pathways during Response Inhibition. J Neurosci 31 Available at: http://www.jneurosci.org/content/31/18/6891.long [Accessed June 28, 2017].

Jansen BH, Rit VG (1995) Electroencephalogram and visual evoked potential generation in a mathematical model of coupled cortical columns. Biol Cybern 73:357–366 Available at: http://link.springer.com/10.1007/BF00199471 [Accessed July 4, 2016].

Jenkinson N, Brown P (2011) New insights into the relationship between dopamine, beta oscillations and motor function. Trends Neurosci 34:611–618.

Karabanov A, Thielscher A, Siebner HR (2016) Transcranial brain stimulation: Closing the loop between brain and stimulation. Curr Opin Neurol 29:397–404.

Khanna P, Carmena JM (2015) Neural oscillations: beta band activity across motor networks. Curr Opin Neurobiol 32:60–67 Available at: http://www.sciencedirect.com/science/article/pii/S0959438814002360 [Accessed October 13, 2015].

Khanna P, Carmena JM (2017) Beta band oscillations in motor cortex reflect neural population signals that delay movement onset. Elife 6 Available at: https://elifesciences.org/articles/24573 [Accessed December 2, 2019].

Kumar A, Cardanobile S, Rotter S, Aertsen A (2011) The role of inhibition in generating and controlling Parkinson's disease oscillations in the Basal Ganglia. Front Syst Neurosci 5:86 Available at: http://journal.frontiersin.org/article/10.3389/fnsys.2011.00086/abstract [Accessed July 19, 2017].

Lalo E, Thobois S, Sharott A, Polo G, Mertens P, Pogosyan A, Brown P (2008) Patterns of Bidirectional Communication between Cortex and Basal Ganglia during Movement in Patients with Parkinson Disease. J Neurosci 28 Available at: http://www.jneurosci.org/content/28/12/3008.long [Accessed November 23, 2016].

Leblois A, Boraud T, Meissner W, Bergman H, Hansel D (2006) Competition between Feedback Loops Underlies Normal and Pathological Dynamics in the Basal Ganglia. J Neurosci 26:3567–3583 Available at: http://www.jneurosci.org/content/26/13/3567.long [Accessed April 26, 2017].

Lee SH, Dan Y (2012) Neuromodulation of Brain States. Neuron 76:209–222.

Levy R (2002) Dependence of subthalamic nucleus oscillations on movement and dopamine in

Parkinson's disease. Brain 125:1196–1209 Available at: http://brain.oxfordjournals.org/content/125/6/1196.abstract [Accessed October 8, 2015].

Liepe J, Kirk P, Filippi S, Toni T, Barnes CP, Stumpf MPH (2014) A framework for parameter estimation and model selection from experimental data in systems biology using approximate Bayesian computation. Nat Protoc 9:439–456 Available at: http://www.nature.com/articles/nprot.2014.025 [Accessed May 13, 2019].

Little S, Bonaiuto J, Barnes G, Bestmann S (2019) Human motor cortical beta bursts relate to movement planning and response errors Ganguly K, ed. PLOS Biol 17:e3000479 Available at: http://dx.plos.org/10.1371/journal.pbio.3000479 [Accessed November 22, 2019].

Little S, Pogosyan A, Neal S, Zavala B, Zrinzo L, Hariz M, Foltynie T, Limousin P, Ashkan K, FitzGerald J, Green AL, Aziz TZ, Brown P (2013) Adaptive deep brain stimulation in advanced Parkinson disease. Ann Neurol 74:449–457 Available at: http://doi.wiley.com/10.1002/ana.23951 [Accessed September 12, 2018].

Litvak V, Jha A, Eusebio A, Oostenveld R, Foltynie T, Limousin P, Zrinzo L, Hariz MI, Friston K, Brown P (2011) Resting oscillatory cortico-subthalamic connectivity in patients with Parkinson's disease. Brain 134:359–374 Available at: http://brain.oxfordjournals.org/content/134/2/359 [Accessed October 14, 2015].

Liu C, Zhu Y, Liu F, Wang J, Li H, Deng B, Fietkiewicz C, Loparo KA (2017) Neural mass models describing possible origin of the excessive beta oscillations correlated with Parkinsonian state. Neural Networks 88:65–73 Available at: http://linkinghub.elsevier.com/retrieve/pii/S0893608017300114 [Accessed August 12, 2017].

Llinás RR, Ribary U, Jeanmonod D, Kronberg E, Mitra PP (1999) Thalamocortical dysrhythmia: A neurological and neuropsychiatric syndrome characterized by magnetoencephalography. Proc Natl Acad Sci U S A 96:15222–15227.

Lundqvist M, Rose J, Herman P, Brincat SL, Buschman TJ, Miller EK (2016) Gamma and Beta Bursts Underlie Working Memory. Neuron 90:152–164 Available at: https://www.sciencedirect.com/science/article/pii/S0896627316001458 [Accessed September 9, 2019].

Magill PJ, Pogosyan A, Sharott A, Csicsvari J, Bolam JP, Brown P (2006) Changes in functional connectivity within the rat striatopallidal axis during global brain activation in vivo. J Neurosci 26:6318–6329 Available at: http://www.ncbi.nlm.nih.gov/sites/entrez?Db=pubmed&DbFrom=pubmed&Cmd=Link&LinkName=pubmed_pubmed&LinkReadableName=Related

Articles&IdsFromResult=16763040&ordinalpos=3&itool=EntrezSystem2.PEntrez.Pubmed.Pubmed_ResultsPanel.Pubmed_RVDocSum [Accessed October 11, 2016].

Magill PJ, Sharott A, Bolam JP, Brown P (2004) Brain State–Dependency of Coherent Oscillatory Activity in the Cerebral Cortex and Basal Ganglia of the Rat. J Neurophysiol 92:2122–2136 Available at: http://jn.physiology.org/content/92/4/2122.full [Accessed April 26, 2017].

Mallet N, Pogosyan A, Marton LF, Bolam JP, Brown P, Magill PJ (2008a) Parkinsonian Beta Oscillations in the External Globus Pallidus and Their Relationship with Subthalamic Nucleus Activity. J Neurosci 28:14245–14258 Available at: http://www.jneurosci.org/cgi/doi/10.1523/JNEUROSCI.4199-08.2008 [Accessed September 5, 2016].

Mallet N, Pogosyan A, Sharott A, Csicsvari J, Bolam JP, Brown P, Magill PJ (2008b) Disrupted Dopamine Transmission and the Emergence of Exaggerated Beta Oscillations in Subthalamic Nucleus and Cerebral Cortex. J Neurosci 28:4795–4806 Available at: http://www.jneurosci.org/cgi/doi/10.1523/JNEUROSCI.0123-08.2008 [Accessed August 5, 2016].

Marreiros AC, Cagnan H, Moran RJ, Friston KJ, Brown P (2013) Basal ganglia–cortical interactions in Parkinsonian patients. Neuroimage 66:301–310 Available at: http://www.sciencedirect.com/science/article/pii/S1053811912010920 [Accessed September 9, 2015].

Martin DM, Liu R, Alonzo A, Green M, Loo CK (2014) Use of transcranial direct current stimulation (tDCS) to enhance cognitive training: effect of timing of stimulation. Exp Brain Res 232:3345–3351.

Mastro KJ, Gittis AH (2015) Striking the Right Balance: Cortical Modulation of the Subthalamic Nucleus-Globus Pallidus Circuit. Neuron 85:233–235 Available at: https://www.sciencedirect.com/science/article/pii/S0896627314011714 [Accessed July 17, 2019].

Mathai A, Ma Y, Paré J-F, Villalba RM, Wichmann T, Smith Y (2015a) Reduced cortical innervation of the subthalamic nucleus in MPTP-treated parkinsonian monkeys. Brain 138:946–962 Available at: http://www.ncbi.nlm.nih.gov/pubmed/25681412 [Accessed July 17, 2019].

Mathai A, Ma Y, Paré J-F, Villalba RM, Wichmann T, Smith Y (2015b) Reduced cortical innervation of the subthalamic nucleus in MPTP-treated parkinsonian monkeys. Brain 138:946–962 Available at: https://academic.oup.com/brain/article-lookup/doi/10.1093/brain/awv018 [Accessed September 4, 2018].

McCarthy MM, Moore-Kochlacs C, Gu X, Boyden ES, Han X, Kopell N (2011) Striatal origin of the pathologic beta oscillations in Parkinson's disease. Proc Natl Acad Sci U S A 108:11620–11625 Available at: http://www.ncbi.nlm.nih.gov/pubmed/21697509 [Accessed April 25, 2017].

McIntyre CC, Hahn PJ (2010) Network perspectives on the mechanisms of deep brain stimulation. Neurobiol Dis 38:329–337.

Moran A, Stein E, Tischler H, Bar-Gad I (2012) Decoupling neuronal oscillations during subthalamic nucleus stimulation in the parkinsonian primate. Neurobiol Dis 45:583–590 Available at: https://www-sciencedirect-com.libproxy.ucl.ac.uk/science/article/pii/S0969996111003299 [Accessed October 31, 2019].

Moran RJ, Mallet N, Litvak V, Dolan RJ, Magill PJ, Friston KJ, Brown P (2011) Alterations in brain connectivity underlying beta oscillations in parkinsonism Kording KP, ed. PLoS Comput Biol 7:e1002124 Available at: http://dx.plos.org/10.1371/journal.pcbi.1002124 [Accessed August 8, 2016].

Palmer C et al. (2016) A New Framework to Explain Sensorimotor Beta Oscillations. Trends Cogn Sci 20:321–323 Available at: http://linkinghub.elsevier.com/retrieve/pii/S136466131600070X [Accessed September 14, 2016].

Pavlides A, Hogan SJ, Bogacz R (2015) Computational Models Describing Possible Mechanisms for Generation of Excessive Beta Oscillations in Parkinson's Disease. PLOS Comput Biol 11:e1004609 Available at: http://dx.plos.org/10.1371/journal.pcbi.1004609.

Paxinos G, Watson C (2007) The rat brain in stereotaxic coordinates. Elsevier.

Peles O, Werner-Reiss U, Bergman H, Israel Z, Vaadia E (2019) Phase-specific microstimulation in brain machine interface setting differentially modulates beta oscillations and affects behavior. bioRxiv:622787 Available at: https://www.biorxiv.org/content/10.1101/622787v1.abstract [Accessed July 23, 2019].

Pirulli C, Fertonani A, Miniussi C (2013) The role of timing in the induction of neuromodulation in perceptual learning by transcranial electric stimulation. Brain Stimul 6:683–689.

Polanía R, Nitsche MA, Korman C, Batsikadze G, Paulus W (2012) The importance of timing in segregated theta phase-coupling for cognitive performance. Curr Biol 22:1314–1318 Available at: http://www.ncbi.nlm.nih.gov/pubmed/22683259 [Accessed November 4, 2019].

Raichle ME (2011) The Restless Brain. Brain Connect 1:3–12 Available at: http://www.liebertpub.com/doi/10.1089/brain.2011.0019 [Accessed September 13, 2018].

Reinhart RMG, Nguyen JA (2019) Working memory revived in older adults by synchronizing

rhythmic brain circuits. Nat Neurosci 22:820–827 Available at: http://www.nature.com/articles/s41593-019-0371-x [Accessed May 31, 2019].

Reis C, Sharott A, Magill PJ, van Wijk BCM, Parr T, Zeidman P, Friston KJ, Cagnan H (2019) Thalamocortical dynamics underlying spontaneous transitions in beta power in Parkinsonism. Neuroimage 193:103–114 Available at: https://www.sciencedirect.com/science/article/pii/S1053811919301764 [Accessed March 26, 2019].

Rosenblum M, Pikovsky A (2004) Delayed feedback control of collective synchrony: An approach to suppression of pathological brain rhythms. Phys Rev E - Stat Physics, Plasmas, Fluids, Relat Interdiscip Top 70:11.

Sanabria DE, Johnson LA, Yu Y, Busby Z, Nebeck S, Zhang J, Harel N, Johnson MD, Molnar GF, Vitek JL (2020) Suppressing and amplifying neural oscillations in real-time using phase-locked electrical stimulation: concept, optimization and in-vivo testing. bioRxiv:2020.02.09.940643.

Schnitzler A, Gross J (2005) Normal and pathological oscillatory communication in the brain. Nat Rev Neurosci 6:285–296 Available at: http://www.nature.com/nrn/journal/v6/n4/execsumm/nrn1650.html [Accessed July 27, 2015].

Sharott A, Gulberti A, Hamel W, Köppen JA, Münchau A, Buhmann C, Pötter-Nerger M, Westphal M, Gerloff C, Moll CKE, Engel AK (2018) Spatio-temporal dynamics of cortical drive to human subthalamic nucleus neurons in Parkinson's disease. Neurobiol Dis 112:49–62 Available at: https://www-sciencedirect-com.libproxy.ucl.ac.uk/science/article/pii/S0969996118300019 [Accessed October 12, 2018].

Sharott A, Magill PJ, Harnack D, Kupsch A, Meissner W, Brown P (2005) Dopamine depletion increases the power and coherence of beta-oscillations in the cerebral cortex and subthalamic nucleus of the awake rat. Eur J Neurosci 21:1413–1422 Available at: http://doi.wiley.com/10.1111/j.1460-9568.2005.03973.x [Accessed September 23, 2016].

Sharott A, Vinciati F, Nakamura KC, Magill PJ (2017) A Population of Indirect Pathway Striatal Projection Neurons Is Selectively Entrained to Parkinsonian Beta Oscillations. J Neurosci 37:9977–9998 Available at: http://www.ncbi.nlm.nih.gov/pubmed/28847810 [Accessed November 24, 2017].

Sherman MA, Lee S, Law R, Haegens S, Thorn CA, Hämäläinen MS, Moore CI, Jones SR (2016) Neural mechanisms of transient neocortical beta rhythms: Converging evidence from humans, computational modeling, monkeys, and mice. Proc Natl Acad Sci U S A 113:E4885-94 Available at: http://www.ncbi.nlm.nih.gov/pubmed/27469163 [Accessed December 2, 2019].

Shin H, Law R, Tsutsui S, Moore CI, Jones SR (2017) The rate of transient beta frequency events predicts behavior across tasks and species. Elife 6 Available at: https://elifesciences.org/articles/29086 [Accessed March 25, 2019].

Shouno O, Tachibana Y, Nambu A, Doya K (2017) Computational Model of Recurrent Subthalamo-Pallidal Circuit for Generation of Parkinsonian Oscillations. Front Neuroanat 11:21 Available at: http://www.ncbi.nlm.nih.gov/pubmed/28377699 [Accessed May 26, 2017].

Siegle JH, Wilson MA (2014) Enhancement of encoding and retrieval functions through theta phase-specific manipulation of hippocampus. Elife 3 Available at: https://elifesciences.org/articles/03061 [Accessed December 2, 2019].

Silvanto J, Muggleton N, Walsh V (2008) State-dependency in brain stimulation studies of perception and cognition. Trends Cogn Sci 12:447–454.

Sirota A, Montgomery S, Fujisawa S, Isomura Y, Zugaro M, Buzsáki G (2008) Entrainment of Neocortical Neurons and Gamma Oscillations by the Hippocampal Theta Rhythm. Neuron 60:683–697 Available at: https://www.sciencedirect.com/science/article/pii/S0896627308007629 [Accessed February 21, 2015].

Stagg CJ, Jayaram G, Pastor D, Kincses ZT, Matthews PM, Johansen-Berg H (2011) Polarity and timing-dependent effects of transcranial direct current stimulation in explicit motor learning. Neuropsychologia 49:800–804.

Steriade M (2000) Corticothalamic resonance, states of vigilance and mentation. Neuroscience 101:243–276.

Tachibana Y, Iwamuro H, Kita H, Takada M, Nambu A (2011) Subthalamo-pallidal interactions underlying parkinsonian neuronal oscillations in the primate basal ganglia. Eur J Neurosci 34:1470–1484 Available at: http://doi.wiley.com/10.1111/j.1460-9568.2011.07865.x [Accessed February 15, 2017].

Tass PA (2000) Stochastic Phase Resetting: A Theory for Deep Brain Stimulation. Prog Theor Phys Suppl 139:301–313 Available at: https://academic.oup.com/ptps/article-lookup/doi/10.1143/PTPS.139.301 [Accessed February 25, 2020].

Terman D, Rubin JE, Yew AC, Wilson CJ (2002) Activity patterns in a model for the subthalamopallidal network of the basal ganglia. J Neurosci 22:2963–2976.

Thut G, Miniussi C, Gross J (2012) The functional importance of rhythmic activity in the brain. Curr Biol 22:R658-63 Available at: http://www.ncbi.nlm.nih.gov/pubmed/22917517 [Accessed

November 15, 2016].

Tinkhauser G, Pogosyan A, Little S, Beudel M, Herz DM, Tan H, Brown P (2017a) The modulatory effect of adaptive deep brain stimulation on beta bursts in Parkinson's disease. Brain 140:1053–1067 Available at: https://academic.oup.com/brain/article/140/4/1053/2993763 [Accessed August 17, 2018].

Tinkhauser G, Pogosyan A, Tan H, Herz DM, Kühn AA, Brown P (2017b) Beta burst dynamics in Parkinson's disease OFF and ON dopaminergic medication. Brain 140:2968–2981 Available at: https://academic.oup.com/brain/article/140/11/2968/4430808 [Accessed April 26, 2018].

Tinkhauser G, Torrecillos F, Duclos Y, Tan H, Pogosyan A, Fischer P, Carron R, Welter M-L, Karachi C, Vandenberghe W, Nuttin B, Witjas T, Régis J, Azulay J-P, Eusebio A, Brown P (2018) Beta burst coupling across the motor circuit in Parkinson's disease. Neurobiol Dis 117:217–225 Available at: https://linkinghub.elsevier.com/retrieve/pii/S0969996118301827.

Torrecillos F, Tinkhauser G, Fischer P, Green AL, Aziz TZ, Foltynie T, Limousin P, Zrinzo L, Ashkan K, Brown P, Tan H (2018) Modulation of Beta Bursts in the Subthalamic Nucleus Predicts Motor Performance. J Neurosci 38:8905–8917 Available at: http://www.jneurosci.org/content/38/41/8905.abstract [Accessed March 14, 2019].

Tye KM, Deisseroth K (2012) Optogenetic investigation of neural circuits underlying brain disease in animal models. Nat Rev Neurosci 13:251–266 Available at: https://doi.org/10.1038/nrn3171.

Uhlhaas PJ, Singer W (2006) Neural Synchrony in Brain Disorders: Relevance for Cognitive Dysfunctions and Pathophysiology. Neuron 52:155–168 Available at: http://www.cell.com/article/S0896627306007276/abstract [Accessed February 21, 2015].

van Albada SJ, Gray RT, Drysdale PM, Robinson PA (2009) Mean-field modeling of the basal ganglia-thalamocortical system. II. Dynamics of parkinsonian oscillations. J Theor Biol 257:664–688.

van Wijk BCM, Beek PJ, Daffertshofer A (2012) Neural synchrony within the motor system: what have we learned so far? Front Hum Neurosci 6:252 Available at: http://journal.frontiersin.org/article/10.3389/fnhum.2012.00252/abstract [Accessed November 15, 2016].

van Wijk BCM, Cagnan H, Litvak V, Kühn AA, Friston KJ (2018) Generic dynamic causal modelling: An illustrative application to Parkinson's disease. Neuroimage 181:818–830 Available at: https://www.sciencedirect.com/science/article/pii/S1053811918307377?via%3Dihub [Accessed November 13, 2018].

Varela F, Lachaux J-PP, Rodriguez E, Martinerie J (2001) The brainweb: phase synchronization and large-scale integration. Nat Rev Neurosci 2:229–239 Available at: http://dx.doi.org/10.1038/35067550 [Accessed October 18, 2014].

Vinck M, van Wingerden M, Womelsdorf T, Fries P, Pennartz CMA (2010) The pairwise phase consistency: A bias-free measure of rhythmic neuronal synchronization. Neuroimage 51:112–122 Available at: http://dx.doi.org/10.1016/j.neuroimage.2010.01.073.

Volkmann J et al. (2009) Long-term effects of pallidal or subthalamic deep brain stimulation on quality of life in Parkinson's disease. Mov Disord 24:1154–1161 Available at: https://onlinelibrary.wiley.com/doi/abs/10.1002/mds.22496.

Wang Y-Y, Wang Y, Jiang H-F, Liu J-H, Jia J, Wang K, Zhao F, Luo M-H, Luo M-M, Wang X-M (2018) Impaired glutamatergic projection from the motor cortex to the subthalamic nucleus in 6-hydroxydopamine-lesioned hemi-parkinsonian rats. Exp Neurol 300:135–148 Available at: https://www.sciencedirect.com/science/article/pii/S0014488617302972 [Accessed December 16, 2019].

Weerasinghe G, Duchet B, Cagnan H, Brown P, Bick C, Bogacz R (2019) Predicting the effects of deep brain stimulation using a reduced coupled oscillator model. PLoS Comput Biol 15:e1006575.

Weinberger M, Mahant N, Hutchison WD, Lozano AM, Moro E, Hodaie M, Lang AE, Dostrovsky JO (2006) Beta oscillatory activity in the subthalamic nucleus and its relation to dopaminergic response in Parkinson's disease. J Neurophysiol 96:3248–3256 Available at: http://jn.physiology.org/content/96/6/3248.short [Accessed September 4, 2015].

West T, Farmer S, Berthouze L, Jha A, Beudel M, Foltynie T, Limousin P, Zrinzo L, Brown P, Litvak V (2016) The Parkinsonian Subthalamic Network: Measures of Power, Linear, and Non-linear Synchronization and their Relationship to L-DOPA Treatment and OFF State Motor Severity. Front Hum Neurosci 10:517 Available at: http://journal.frontiersin.org/article/10.3389/fnhum.2016.00517/full [Accessed October 7, 2016].

West TO, Berthouze L, Farmer SF, Cagnan H, Litvak V (2019a) Mechanistic Inference of Brain Network Dynamics with Approximate Bayesian Computation. bioRxiv:785568 Available at: https://www.biorxiv.org/content/10.1101/785568v2 [Accessed October 14, 2019].

West TO, Berthouze L, Halliday DM, Litvak V, Sharott A, Magill PJ, Farmer SF (2018) Propagation of Beta/Gamma Rhythms in the Cortico-Basal Ganglia Circuits of the Parkinsonian Rat. J Neurophysiol:jn.00629.2017 Available at: http://www.physiology.org/doi/10.1152/jn.00629.2017 [Accessed April 20, 2018].

West TO, Halliday DM, Bressler S, Farmer SF, Litvak V (2019b) Measuring directed functional connectivity in neural data using Non-Parametric Directionality Analysis: validation and comparison with Non-Parametric Granger Causality. bioRxiv:526566 Available at: https://www.biorxiv.org/content/10.1101/526566v1 [Accessed April 10, 2019].

Williams D, Tijssen M, Van Bruggen G, Bosch A, Insola A, Di Lazzaro V, Mazzone P, Oliviero A, Quartarone A, Speelman H, Brown P (2002) Dopamine-dependent changes in the functional connectivity between basal ganglia and cerebral cortex in humans. Brain 125:1558–1569.

Womelsdorf T, Schoffelen J-M, Oostenveld R, Singer W, Desimone R, Engel AK, Fries P (2007) Modulation of Neuronal Interactions Through Neuronal Synchronization. Science (80-) 316:1609 LP – 1612 Available at: http://science.sciencemag.org/content/316/5831/1609.abstract.

Zanos S, Rembado I, Chen D, Fetz EE (2018) Phase-Locked Stimulation during Cortical Beta Oscillations Produces Bidirectional Synaptic Plasticity in Awake Monkeys. Curr Biol 28:2515-2526.e4 Available at: https://www.sciencedirect.com/science/article/pii/S0960982218309084?via%3Dihub [Accessed June 20, 2019].